Our *in vitro* and *in vivo* analyses indicate that L-PGDS contributes to myelin formation. However, the *in vivo* phenotype was not as severe as the one observed *in vitro*. Whether this is the result of an exacerbation of *in vitro* settings or of compensation from other prostaglandins expressed in the nerves is remains unknown. Our study excludes the possibility that H-PGDS contributes to the phenotype, although it has been reported that other members of the lipocalin family, such as ApoD and ApoE, are important during regeneration following nerve injury[48,49]. Furthermore, it is possible that L-PGDS and Gpr44 act preferentially onto sensory fibers, as suggested by the marked hypomyelination of small fibers in *Gpr44*$^{-/-}$ and increased *g* ratio values in saphenous nerves.

The hypomyelinating phenotype is similar in *L-pgds*$^{-/-}$ and *H-pgds*$^{-/-}$; *L-pgds*$^{-/-}$ mice. However, only in aged *H-pgds*$^{-/-}$; *L-pgds*$^{-/-}$ mice was myelin significantly altered ($P < 0.0001$), suggesting that PGD2 might be important for myelin stability, as supported by *in vitro* studies. Although we observed some fibers with aberrant myelin in 6-month-old *L-pgds*$^{-/-}$ mice, the precise mechanism implicating PGD2 in myelin formation and maintenance remains unclear. Whether L-PGDS and Gpr44 simply stabilize the adhesion at the adaxonal membrane or represent an extra checkpoint for myelination is unknown. Initiation of myelination and the amount of myelin formed depends on NRG1 type III forward signaling, although it is possible that L-PGDS, activated by NRG1 itself, signals back to Schwann cells to stabilize myelin. In the absence of L-PGDS, this checkpoint is lacking and the myelin formed is unstable, resulting in fast and continuous remodeling. Alternatively, L-PGDS and Gpr44 could be part of a feedback mechanism by which the axon is communicating to Schwann cells its integrity, indicating that myelination can continue. We favor the latter hypothesis, as hypomyelination in older animals was accompanied by severe myelin alterations, but not axonal suffering, suggesting that, in *L-pgds*$^{-/-}$ mice, Schwann cells might not recognize the axon as intact despite NRG1 type III forward signaling. Whether the myelin damage is the result of myelin instability or the lack of continuous communication is currently unknown. We cannot exclude the possibility that L-PGDS exerts both functions. In future studies, it will be particularly important to determine how neuronal specific ablation of L-PGDS *in vivo* in adults affects myelin stability.

The use of agonists enhancing L-PGDS enzymatic activity, the transduction capability of Gpr44 or both could constitute a new approach to treating peripheral demyelinating neuropathies. Furthermore, as this pathway might be involved in myelin maintenance, activation of prostaglandins could be particularly efficacious for the treatment of demyelinating disorders with late onset. Notably, specific molecules that have already been developed and whose efficacy has been tested in other biological systems[36] are available and could pharmacologically target this level of communication between glial cells.

In conclusion, we propose that NRG1 type III controls myelination in multiple ways. The canonical forward signal is required to initiate myelination[31] and regulate the amount of myelin formed[50]. The backward signal, by upregulating the expression of L-PGDS, activates a previously unknown pathway that is relevant in PNS myelination and maintenance and whose modulation could be beneficial for the treatment of peripheral demyelinating neuropathies.

METHODS

Methods and any associated references are available in the online version of the paper.

Accession codes. The data discussed in this publication have been deposited in NCBI's Gene Expression Omnibus and are accessible through GEO Series accession number GSE61784.

Note: Any Supplementary Information and Source Data files are available in the online version of the paper.

ACKNOWLEDGMENTS

We thank V. Marzano and A. Urbani for shotgun mass spectrometry analyses, F. Clarelli for heat map and statistical analyses, G. Fitzgerald (University of Pennsylvania) for providing *Gpr44*$^{-/-}$ mice, P. Podini for excellent technical assistance with electron microscopy analyses, and P. Del Boccio for LC-MS/MS analyses. We are grateful to M. Buono, S. Previtali and A. Bolino for critical reading of the manuscript and suggestions, and L. Massimino for artwork. Part of this work was carried out in ALEMBIC, an advanced microscopy laboratory at the San Raffaele Scientific Institute. M.G.F. conducted this study in partial fulfillment for her Ph.D. in Molecular and Cellular Neuroscience, San Raffaele University. This study was supported by the Italian Minister of Health (award number GR08-35, C.T.), the European Marie Curie Reintegration Grant (award number IRG 239430-2008, C.T.) and the Agence Nationale pour la Recherche (ANR blanc programme, B.B.B.). C.T. is also supported by Italian Fondazione Italiana Sclerosi Multipla.

AUTHOR CONTRIBUTIONS

A.T. designed and conducted the majority of the experiments. M.G.F., V.A. and A.L. contributed to *in vitro* and biochemical studies. P.B. and F.M.B. performed expression studies. G.D. and A.Q. performed morphological and ultrastructural analyses. Y.U. and B.B.-B. provided transgenic lines and provided input. D.P. and P.S. performed the MS/MS-LC analyses. C.T. designed the experimental plan, supervised the project and wrote the manuscript.

COMPETING FINANCIAL INTERESTS

The authors declare competing financial interests: details are available in the online version of the paper.

1. Birchmeier, C. & Nave, K.A. Neuregulin-1, a key axonal signal that drives Schwann cell growth and differentiation. *Glia* **56**, 1491–1497 (2008).
2. Willem, M. *et al.* Control of peripheral nerve myelination by the beta-secretase BACE1. *Science* **314**, 664–666 (2006).
3. Hu, X. *et al.* Bace1 modulates myelination in the central and peripheral nervous system. *Nat. Neurosci.* **9**, 1520–1525 (2006).
4. La Marca, R. *et al.* TACE (ADAM17) inhibits Schwann cell myelination. *Nat. Neurosci.* **14**, 857–865 (2011).
5. Bao, J., Wolpowitz, D., Role, L.W. & Talmage, D.A. Back signaling by the Nrg-1 intracellular domain. *J. Cell Biol.* **161**, 1133–1141 (2003).
6. Bao, J. *et al.* Activity-dependent transcription regulation of PSD-95 by neuregulin-1 and Eos. *Nat. Neurosci.* **7**, 1250–1258 (2004).
7. Chen, Y., Hancock, M.L., Role, L.W. & Talmage, D.A. Intramembranous valine linked to schizophrenia is required for neuregulin 1 regulation of the morphological development of cortical neurons. *J. Neurosci.* **30**, 9199–9208 (2010).
8. Urade, Y. & Eguchi, N. Lipocalin-type and hematopoietic prostaglandin D synthases as a novel example of functional convergence. *Prostaglandins Other Lipid Mediat.* **68–69**, 375–382 (2002).
9. Giacomelli, S., Leone, M.G., Grima, J., Silvestrini, B. & Cheng, C.Y. Astrocytes synthesize and secrete prostaglandin D synthetase *in vitro*. *Biochim. Biophys. Acta* **1310**, 269–276 (1996).
10. Samy, E.T. *et al.* Sertoli cell prostaglandin D2 synthetase is a multifunctional molecule: its expression and regulation. *Endocrinology* **141**, 710–721 (2000).
11. Nagata, N. *et al. De novo* synthesis, uptake and proteolytic processing of lipocalin-type prostaglandin D synthase, beta-trace, in the kidneys. *FEBS J.* **276**, 7146–7158 (2009).
12. Tootle, T.L. Genetic insights into the *in vivo* functions of prostaglandin signaling. *Int. J. Biochem. Cell Biol.* **45**, 1629–1632 (2013).
13. Haskew-Layton, R.E., Payappilly, J.B., Xu, H., Bennett, S.A. & Ratan, R.R. 15-Deoxy-Delta12,14-prostaglandin J2 (15d-PGJ2) protects neurons from oxidative death via an Nrf2 astrocyte-specific mechanism independent of PPARgamma. *J. Neurochem.* **124**, 536–547 (2013).
14. Kerr, B.J., Girolami, E.I., Ghasemlou, N., Jeong, S.Y. & David, S. The protective effects of 15-deoxy-delta-(12,14)-prostaglandin J2 in spinal cord injury. *Glia* **56**, 436–448 (2008).
15. Urade, Y. & Hayaishi, O. Prostaglandin D synthase: structure and function. *Vitam. Horm.* **58**, 89–120 (2000).
16. Kostenis, E. & Ulven, T. Emerging roles of DP and CRTH2 in allergic inflammation. *Trends Mol. Med.* **12**, 148–158 (2006).
17. Beuckmann, C.T. *et al.* Cellular localization of lipocalin-type prostaglandin D synthase (beta-trace) in the central nervous system of the adult rat. *J. Comp. Neurol.* **428**, 62–78 (2000).
18. Kao, S.C. *et al.* Calcineurin/NFAT signaling is required for neuregulin-regulated Schwann cell differentiation. *Science* **323**, 651–654 (2009).
19. Grimwood, S. *et al.* Determination of guinea-pig cortical gamma-secretase activity *ex vivo* following the systemic administration of a gamma-secretase inhibitor. *Neuropharmacology* **48**, 1002–1011 (2005).

20. Beuckmann, C.T. *et al.* Lipocalin-type prostaglandin D synthase (beta-trace) is located in pigment epithelial cells of rat retina and accumulates within interphotoreceptor matrix. *J. Neurosci.* **16**, 6119–6124 (1996).
21. Mohri, I. *et al.* Prostaglandin D2–mediated microglia/astrocyte interaction enhances astrogliosis and demyelination in twitcher. *J. Neurosci.* **26**, 4383–4393 (2006).
22. Subra, C. *et al.* Exosomes account for vesicle-mediated transcellular transport of activatable phospholipases and prostaglandins. *J. Lipid Res.* **51**, 2105–2120 (2010).
23. Irikura, D. *et al.* Biochemical, functional, and pharmacological characterization of AT-56, an orally active and selective inhibitor of lipocalin-type prostaglandin D synthase. *J. Biol. Chem.* **284**, 7623–7630 (2009).
24. Vesin, M.F., Urade, Y., Hayaishi, O. & Droz, B. Neuronal and glial prostaglandin D synthase isozymes in chick dorsal root ganglia: a light and electron microscopic immunocytochemical study. *J. Neurosci.* **15**, 470–476 (1995).
25. Ragolia, L. *et al.* Accelerated glucose intolerance, nephropathy, and atherosclerosis in prostaglandin D2 synthase knock-out mice. *J. Biol. Chem.* **280**, 29946–29955 (2005).
26. Qu, W.M. *et al.* Lipocalin-type prostaglandin D synthase produces prostaglandin D2 involved in regulation of physiological sleep. *Proc. Natl. Acad. Sci. USA* **103**, 17949–17954 (2006).
27. Kanekiyo, T. *et al.* Lipocalin-type prostaglandin D synthase/beta-trace is a major amyloid beta-chaperone in human cerebrospinal fluid. *Proc. Natl. Acad. Sci. USA* **104**, 6412–6417 (2007).
28. Moniot, B. *et al.* The PGD2 pathway, independently of FGF9, amplifies SOX9 activity in Sertoli cells during male sexual differentiation. *Development* **136**, 1813–1821 (2009).
29. Raff, M.C., Abney, E., Brockes, J.P. & Hornby-Smith, A. Schwann cell growth factors. *Cell* **15**, 813–822 (1978).
30. Monje, P.V., Athauda, G. & Wood, P.M. Protein kinase A–mediated gating of neuregulin-dependent ErbB2-ErbB3 activation underlies the synergistic action of cAMP on Schwann cell proliferation. *J. Biol. Chem.* **283**, 34087–34100 (2008).
31. Taveggia, C. *et al.* Neuregulin-1 type III determines the ensheathment fate of axons. *Neuron* **47**, 681–694 (2005).
32. Ogata, T. *et al.* Opposing extracellular signal–regulated kinase and Akt pathways control Schwann cell myelination. *J. Neurosci.* **24**, 6724–6732 (2004).
33. Newbern, J.M. *et al.* Specific functions for ERK/MAPK signaling during PNS development. *Neuron* **69**, 91–105 (2011).
34. Lal, M. & Caplan, M. Regulated intramembrane proteolysis: signaling pathways and biological functions. *Physiology (Bethesda)* **26**, 34–44 (2011).
35. Harizi, H. The immunobiology of prostanoid receptor signaling in connecting innate and adaptive immunity. *Biomed. Res. Int.* **2013**, 683405 (2013).
36. Taketomi, Y. *et al.* Mast cell maturation is driven via a group III phospholipase A2-prostaglandin D2–DP1 receptor paracrine axis. *Nat. Immunol.* **14**, 554–563 (2013).
37. Tin, A. *et al.* Genome-wide significant locus of beta-trace protein, a novel kidney function biomarker, identified in European and African Americans. *Nephrol. Dial. Transplant.* **28**, 1497–1504 (2013).
38. Greenberg, M.E., Xu, B., Lu, B. & Hempstead, B.L. New insights in the biology of BDNF synthesis and release: implications in CNS function. *J. Neurosci.* **29**, 12764–12767 (2009).
39. Evans, S.F. *et al.* Neuronal brain-derived neurotrophic factor is synthesized in excess, with levels regulated by sortilin-mediated trafficking and lysosomal degradation. *J. Biol. Chem.* **286**, 29556–29567 (2011).
40. Nicholson, J.D. *et al.* PGJ(2) provides prolonged CNS stroke protection by reducing white matter edema. *PLoS ONE* **7**, e50021 (2012).
41. Kipanyula, M.J. *et al.* Calcineurin-nuclear factor of activated T cells regulation of Krox-20 expression in Schwann cells requires elevation of intracellular cyclic AMP. *J. Neurosci. Res.* **91**, 105–115 (2013).
42. Hirahara, Y. *et al.* G protein-coupled receptor 30 contributes to improved remyelination after cuprizone-induced demyelination. *Glia* **61**, 420–431 (2013).
43. Hennen, S. *et al.* Decoding signaling and function of the orphan G protein–coupled receptor GPR17 with a small-molecule agonist. *Sci. Signal.* **6**, ra93 (2013).
44. Monk, K.R. *et al.* A G protein–coupled receptor is essential for Schwann cells to initiate myelination. *Science* **325**, 1402–1405 (2009).
45. Monk, K.R., Oshima, K., Jors, S., Heller, S. & Talbot, W.S. Gpr126 is essential for peripheral nerve development and myelination in mammals. *Development* **138**, 2673–2680 (2011).
46. Glenn, T.D. & Talbot, W.S. Analysis of Gpr126 function defines distinct mechanisms controlling the initiation and maturation of myelin. *Development* **140**, 3167–3175 (2013).
47. Mogha, A. *et al.* Gpr126 functions in Schwann cells to control differentiation and myelination via G-protein activation. *J. Neurosci.* **33**, 17976–17985 (2013).
48. Ganfornina, M.D. *et al.* ApoD, a glia-derived apolipoprotein, is required for peripheral nerve functional integrity and a timely response to injury. *Glia* **58**, 1320–1334 (2010).
49. Comley, L.H. *et al.* ApoE isoform–specific regulation of regeneration in the peripheral nervous system. *Hum. Mol. Genet.* **20**, 2406–2421 (2011).
50. Michailov, G.V. *et al.* Axonal neuregulin-1 regulates myelin sheath thickness. *Science* **304**, 700–703 (2004).

ONLINE METHODS

Mice and genotyping. Generation of *H-pgds*$^{-/-}$; *L-pgds*$^{-/-}$ mice has been described previously[51,52]. *H-pgds*$^{-/-}$; *L-pgds*$^{-/-}$ mice were obtained in Mendelian ratio, by crossing *H-pgds*$^{+/-}$ and *L-pgds*$^{+/-}$ mice. All experiments were performed on animals of both sexes in a C57/Bl6 congenic background. Mice were genotyped by PCR using the following primers. Wild-type alleles: 5′-GAGTTGCTGCATCTGACCTTTTC-3′ and 5′-TAGCGAATAATTTCGG CTCTTCC-3′; *H-PGDS*: (773 bp) and 5′-TGTCAGGAATGTGGTATGCTC-3′ and 5′-AATACAGCTTTCTTCTCCCGGAAC-3′; *L-PGDS*: (338 bp) and the following PCR cycling conditions: 95 °C for 30 s, 52 °C for 30 s and 72 °C for 60 s (30 cycles). *H-PGDS*$^{-/-}$: 5′-ATCGCCTTCTATCGCCTTCTTGACGAGT-3′ and 5′-ATGTGTACTGGCTCCAACTTCCCAGAGAGT-3′ (800 bp); *L-PGDS*$^{-/-}$: 5′-TCTTGAGAGTGCAACAGAGCAAAGGAGTCC-3′ and 5′-ATCGCCTTCT ATCGCCTTCTTGACGAGT-3′ (650 bp) and the following PCR cycling conditions: 95 °C for 30 s, 60 °C for 30 s and 72 °C for 60 s (30 cycles).

Generation of *Gpr44*$^{-/-}$ has been previously described[53]. *Gpr44*$^{-/-}$ were genotyped by PCR using the following primers. 5′-CTCGCCGGACACGCT GAACTTGT-3′, 5′-TGGGGTCAAACTCAGCTCCTCACG-3′, and 5′-GCG GCGGCTAA CAAGTCGGATAG-3′ with the following PCR cycling conditions: 93 °C for 30 s, 55 °C for 30 s and 72 °C for 180 s (35 cycles). All amplified fragments were analyzed on a 1.5% agarose gel. All experiments involving animals followed protocols approved by the Animal Care and Use Committee of San Raffaele Scientific Institute.

Constructs. Full-length NRG1 type III lentivirus (pL6/V5 NRG1) was generated as described[31]. The C-NRG1 plasmid was obtained by cloning the *EGFP* cDNA in frame into the unique Xho I restriction site of pL6/V5 NRG1. *Nrg1* stop codon and *EGFP* ATG were mutated by standard PCR mutagenesis. N-NRG1 was obtained by standard PCR mutagenesis by cloning the *EGFP* sequence in frame and without its ATG between aminoacid 26 and 27 of NRG1 type III cDNA, to avoid interference with putative NRG1 signal peptide.

NRG1 ICD–EGFP was obtained by cloning the intracellular domain of rat NRG1 type III, from K 1020 to V 2100, without the stop codon, in the *pL6/V5* plasmid by topoisomerase. Upstream K1020 we inserted an ATG by standard PCR mutagenesis. The *EGFP* cDNA was cloned in frame into the unique Xho I restriction site of pL6/V5 NRG1-ICD. *Nrg1* stop codon and *EGFP* ATG were mutated by standard PCR mutagenesis.

NRG1 type III–FLAG and NRG1 ICD–FLAG plasmids were obtained by replacing the *EGFP* epitope into C-NRG1 and NRG1 ICD–EGFP with the 3XFLAG epitope. The 3XFLAG epitope was amplified by PCR from the p3X-FLAG-CMV-14 expression vector (Sigma Aldrich). Specifically, we introduced the XhoI and SacII restriction sites in the p3XFLAG-CMV-14 vector upstream and downstream the *3XFLAG* sequence respectively by PCR mutagenesis.

Rat *L-PGDS* cDNA was amplified by PCR from brain mRNA and cloned into the pL6/V5 plasmid in the Spe I and Sac II restriction sites. All constructs were obtained following standard molecular biology techniques and confirmed by sequencing.

Cell cultures. Mouse and rat DRG neurons were isolated from E14.5 or E16.5 embryos and established on collagen-coated glass coverslips as described[31]. Explants were cycled either with FUDR to eliminate all non-neuronal cells or in some experiments endogenous Schwann cells were maintained. Neuronal media was supplemented with 50 ng ml^{-1} NGF (Harlan, Bioproducts for Science). Primary rat Schwann cells were prepared as described[31] and maintained in DMEM (Invitrogen), 10% FBS (vol/vol, Invitrogen), 2 mM L-glutamine (Invitrogen), until used. Rat Schwann cells were added (200,000 cells per coverslip) to establish explant cultures of DRG neurons and myelination was initiated by supplementing media with 50 μg ml^{-1} ascorbic acid (Sigma–Aldrich).

In some experiments, purified DRG neurons, Schwann cell–DRG neuronal co-cultures or isolated Schwann cells were treated with various concentrations of AT-56 (Cayman Chemicals), 5, 10, 25 and 50 μM 15R-methyl-prostaglandin D2 (Cayman Chemicals), 10 μM Compound E (EMD Millipore) both dissolved in DMSO (Sigma Aldrich), 10 nM cyclosporin A (Novartis), 100 nM recombinant PGD2 dissolved in ethanol (Cayman Chemicals), 2.5 μM Forskolin (Sigma Aldrich), 2.5 ng ml^{-1} recombinant human NRG1β1 (EGF domain, R&D).

Lentiviral production and infection. Individual shRNA clones (TRCN0000027873: shA3; TRCN0000027876: shA5; TRCN0000027894: shC9) specifically targeting mouse *Gpr44* were obtained through the RNAi Consortium (Open Biosystem/Thermoscientific). Lentiviral vectors, *Gpr44* shRNA and scramble shRNA were transfected into 293FT cells (Invitrogen) and viruses were produced as described[4]. Viral supernatants were collected and stored as described[4]. Freshly plated Schwann cells (10^6 cells per 100-mm plate) were incubated for 2 d with *Gpr44* shRNA lentiviruses at a 2/3 dilution (vol/vol) in DMEM, 10% FBS and 2 mM D-glutamine supplemented with forskolin and rh NRG-1 (EGF domain, R&D). Cells were expanded for an additional week and maintained for 3 d in Schwann cell media prior seeding. Protein knockdowns were confirmed by qRT-PCR analyses. Mouse and rat DRG neuronal explants were infected the day after the dissection and left in the presence of the virus for 24 h after which cultures were purified of endogenous Schwann cell to obtain pure DRG neurons by cycling them with antimitotic reagents or cultured with endogenous Schwann cell. In the latter case, both DRG neurons and mouse primary Schwann cell were infected.

Electron microscopy and morphological analyses. Semi-thin and ultrathin sections were obtained as described[54]. Tissues were removed and fixed with 2% glutaraldehyde (vol/vol) in 0.12 M phosphate buffer, postfixed with 1% osmium tetroxide (vol/vol), and embedded in Epon (Fluka). Semi-thin sections (0.5–1 μm thick) were stained with toluidine blue and examined by light microscopy (Olympus BX51). Ultrathin sections (70–90 nm thick) were stained with uranile acetate and lead citrate and examined by electron microscopy (Leo 912 Omega). Digitized non-overlapping semi-thin sections images from corresponding levels of the sciatic nerve were obtained with a digital camera (Leica DFC300F) using a 100× objective. *g* ratio measurements were performed on digitized non overlapping electron micrographs images. *g* ratio was determined by dividing the mean diameter of an axon without myelin by the mean diameter of the same axon with myelin. A minimum of 150 randomly chosen fibers per animal were analyzed for *g* ratio measurements at P7, 1 month, 2 months, 6 months, 8 months and 9 months. To determine the size distribution of myelinated fibers in sciatic nerves, diameters of all fibers in at least ten images of randomly chosen representative images were measured and binned based on their width. All measurements were acquired on electron microscopy sections images using an ImageJ software. Data are expressed as the percentage relative to the total number of fibers. Similarly, the number of myelinated fibers per area in sciatic nerves and roots was determined on 100× images acquired on semi-thin sections and analyzed using ImageJ Software. All measurements were blindly performed. Electron microscopy analyses on Schwann cell–DRG neurons myelinating co-cultures were performed as described previously[55].

Microarray analyses. Gene expression study was performed using the Illumina RatRef-12 Expression BeadChips. Each individual array on the chip targets more than 21,000 transcripts selected primarily from the NCBI RefSeq database (Release 16) and in a minor part from the UniGene database. 500 ng of total RNA was reverse transcribed into cRNA (complementary RNA) and biotin-UTP labeled using the Illumina TotalPrep RNA Amplification Kit (Ambion). 750 ng of cRNA in 11 μl (150 ng μl^{-1}) were hybridized to the BeadChip Array at 58 °C overnight. The fluorescent signal was developed through a streptavidin-Cy3 staining step. BeadChips were imaged using the Illumina BeadArray Reader, a two-channel 0.8-μm resolution confocal laser scanner. The software Illumina GenomeStudio version 2011.1 was used to take fluorescent hybridization signals and to assess the system quality controls, such as biological specimen, hybridization, signal generation and negative controls. For each experimental condition four biological replicates have been analyzed, and technical replicates have been tested in 4 of 12 samples. The mean correlation coefficient value of technical replicates was 0.993 (s.d., 0.005) and of biological ones was 0.967 (s.d., 0.013). Sample clustering analysis based on the absolute correlation metric parameter was also performed, and the graphical representation of the dendrogram further supported the technical validity of the data.

Data were $\log_2$ transformed, normalized using the quantile algorithm (R beadarray package) and all probes with a detection $P > 0.01$ in all experimental conditions were excluded from the analyses. For differential expression analysis, a moderated *t* statistics was performed using Limma package in R. Fold change values were also calculated. Transcript probes were classified as differentially

expressed based on a fold change cut-off of 2.0 and $P < 0.01$ considering the following comparisons: lentiviruses expressing NRG1 ICD versus not infected; lentiviruses expressing *EGFP* versus not infected and lentiviruses expressing *NRG1 ICD* versus those expressing only *EGFP*.

Microarray data were deposited in Array Express with the following accession number: E-MTAB-2131. The data discussed in this publication have been deposited in NCBI's Gene Expression Omnibus and are accessible through GEO Series accession number GSE61784.

RNA isolation and measurements. Total RNA was isolated from rat Schwann cells, rat purified DRG neurons and co-cultures using Trizol (Roche), according to manufacturer's instruction. Total RNA was retro-transcribed to cDNA as described[56]. Aliquots of RT products were tested in parallel using primers pair for rat *L-pgds* and *Gapdh*. *L-pgds* primers were: 5′-GAGAAGAAAGAG CTACTGTTTATGTGC-3′ (forward) and 5′-CTAAAGGTGATGAATTTCTC CTTCAG-3′ (reverse). PCR cycling conditions were 94 °C for 30 s, 56 °C for 60 s and 72 °C for 90 s, 24 cycles, followed by 5 min extension at 72 °C. *Gapdh* primers were: 5′-GGTTACCAGGGCTGCCTTCTCTTGTGA-3′ (forward) and 5′-CGGAAGGGGCGGAGATGATGACCCT-3′ (reverse). PCR cycling conditions were: 94 °C for 30 s, 64 °C for 60 s and 72 °C for 90 s, 22 cycles, followed by 5 min extension at 72 °C.

qRT-PCR. PCR analyses were performed using Sso Fast Eva Green Supermix according to manufacturer's instructions. Genes of interest and housekeeping genes were amplified using the same reaction protocol. To test *L-PGDS*, *Nfatc4* and *Sod3* expression we used the following set of primers: *L-pgds*: 5′-GAGAAGAAAGAGCTACTGTTTATGTGC-3′ (forward) and 5′-CTAA AGGTGATGAATTTCTCCTTCAG-3′ (reverse); *Nfatc4* 5′-CAGGTCTACT TTTTATGTCTCCAATGG-3′ (forward) and 5′-ATCCGTAGGCCAGATCT ATAAGACG-3′ (reverse); *Sod3* 5′–TTCTTGTTCTGCAACCTGCTACT-3′ (forward) and 5′-ATTGAAGGAGGCCTCAAGTCTG-3′ (reverse); *Gapdh*: 5′-GGTCTACATGTTCCAGTATGACTCTA-3′ (forward) and 5′-CTTCTTG AGGGAGTTGTCATATTTCTC-3′ (reverse). PCR cycling conditions were 95 °C for 30 s, 56 °C for 60 s 72 °C for 90 s (41 cycles). To test *Ptgdr*, *Pparg* and *Gpr44* expression we used the following primers: *Ptgdr*: 5′-CA TTCTCGGTAATAGGCTTCTCTG-3′ (forward) and 5′-TCCACAAGTTTA AAGGCTCCATAG-3′ (reverse); *Pparg*: 5′-CTGTCGGATCCACAAAAA GAGTAG (forward) and 5′-GAATTCATGTCGTAGATGACAAATG-3′ (reverse); *Gpr44*: 5′-CACTACTCTATGTGCTCACTTGTCC-3′ (forward) and 5′-CCATCTAATCCAAAGTACAGCTCAA-3′ (reverse); *Gapdh*: 5′-ACCTCA ACTACATGGTCTACATGTTC-3′ (forward) and 5′-ATCTTGAGGGAGTT GTCATATTTCTC-3′ (reverse). PCR cycling conditions were: 95 °C for 30 s, 58 °C for 60 s, 72 °C for 90 s (41 cycles).

To determine *L-pgds* expression in mouse DRG–rat Schwann cell co-cultures, we used the primers specific for the mouse sequence that do not amplify the rat gene. *L-pgds*: 5′-GGAGAAGAAAGCTGTATTGTATATGTGC-3′ (forward); 5′-TAAAGGTGGTGAATTTCTCCTTCAG-3′ (reverse); *Gapdh*: 5′-TCACCAGGGCTGCCATTTGCAGTGG-3′ (forward) 5′-CGGAAGGGGC GGAGATGATGACCCT-3′ (reverse). PCR cycling conditions were: 95 °C for 30 s, Tm for 60 s, 72 °C for 60 s (41 cycles). Tm was for 56 °C mouse *L-pgds* and 62 °C for mouse *Gapdh*.

LC-MS/MS analyses. Levels of PGD2 were measured by modifying previously described methods[57] by using a LC-MS/MS system (Waters). Briefly, after adjustment of sample to pH 3 with HCl 2N and incubation with methyloxamine HCl (1 g ml^{-2}) and d_6-PGE-M (40 ng), as internal standard, Cayman Chemical) for 60 min at 25 °C, PGD2 was extracted by using Strata-X 33-μm polymeric reversed phase SPE columns (30 mg ml^{-1}, Phenomenex) and eluted with ethyl acetate and then dried with a Speed-Vac (Speed Vac Plus, Savant Instruments). After dryness, the pellet was resuspended with 50 μl of water/ACN (90/10) and injected into a LC-MS/MS system. The LC-MS/MS system consisted into a Waters Alliance 2795 LC coupled to a Micromass Quattro Pt triple-quadrupole mass spectrometer (TQuattro-Pt, Waters) equipped with a Z-Spray ESI source, operated in negative ion mode. The LC column was a Synergy HydroRP (150 × 1 mm, 4μ) (Phenomenex) maintained at 25 °C. The mobile phase was acetonitrile (solvent A) and water (solvent B) (both added with 0.005% acetic acid, vol/vol) at a flow rate of 0.070 ml min^{-1}.

The gradient timetable was the following: injection at 10% A; 70% A at 25 min; 10% A at 26 min; 10% A at 40 min. The ionization mode was electrospray in negative polarity (ES). The transitions monitored in Multiple Reaction Monitoring (MRM) are 380>186 *m/z* for the endogenous compound PGD2 and 391>342 *m/z* for the internal standard PGEMd6. The collision energy used was 14 eV.

Preparation of detergent lysates and immunoblotting. Tissues and cell lysates were prepared as described[31]. Supernatants were aliquoted and stored at −80 °C until used. Protein concentrations were determined by the BCA method (Pierce); samples (20–40 μg of protein) were fractionated by SDS-PAGE and blotted onto nitrocellulose (Protran Biosciences). Membranes were blocked in 5% BSA, 0.05% sodium azide in TBST (0.1% Triton X-100 in Tris-buffered saline (TBS), vol/vol). Appropriate regions were excised, incubated with specific primary and secondary antibodies, washed in TBST and developed with the SuperSignal chemiluminescent substrate (Pierce). For quantitative western blotting analyses, filters were analyzed using the Odyssey Infrared Imaging System (LI-COR Biosciences) according to manufacturer's instructions.

Tunel and proliferation assays. Both assays were performed as described[58] on three different P2 mice per genotype and four different slides per animal. For proliferation assays, sciatic nerve sections were permeabilized with 0.2% Triton X-100 (vol/vol), blocked with 10% FCS (vol/vol), 0.1 M lysine, and 0.02% sodium azide (vol/vol) in 0.1 M phosphate-buffered saline (PBS), and incubated with a rabbit antibody to PH3 (Millipore). Tunel assay was performed on adjacent sections using the DeadEnd Fluorometric TUNEL System (Promega G3250) according to manufacturer's instructions.

Antibodies and immunofluorescence. All antibodies used were previously validated for the applications used, except for antibody to L-PGDS, which we validated in lysates prepared from *L-pgds*$^{-/-}$ mice, and antibody to H-PGDS, which we confirmed on sciatic nerve cryosections of *H-pgds*$^{-/-}$ mice. Mouse monoclonal antibodies included antibodies to MBP (Covance SMI-94R and SMI-99R, 1:4,000 for western blotting), neurofilament (Covance SMI-31R and SMI-32R, 1:10,000 for western blotting), neuronal class III β-tubulin (TuJ1, Covance MMS-435 1:1,000 for immunofluorescence) and Caspr (NeuroMab clone K65/35, 1:100 for immunohistochemistry). Rabbit polyclonal antibodies included antibodies to actin (Sigma Aldrich A2066, 1:5,000 for western blotting), FLAG (Sigma Aldrich F7425, 1:400 for immunohistochemistry), Calnexin (Sigma-Aldrich, C4731 1:4,000 for western blotting), L-PGDS (Abnova PAB 12054, 1:500 for western blotting), H-PGDS (LSBio LS-B6886/48259, 1:200 for immunofluorescence), S100 beta (DakoCytomation Z0311, 1:200 for immunofluorescence), phospho-AKT (ser 473) (Cell Signaling Technology 4060, 1:1,000 for western blotting), total AKT (Cell Signaling Technology 4691, 1:1,000 for western blotting), phospho-ERK (p44, p42) (Cell Signaling Technology 9101, 1:1,000 for western blotting), total ERK (Cell Signaling Technology 9102, 1:1,000 for western blotting), Nfat3 (Cell Signaling Technology 2183, 1:500 for western blotting), phospho-PKA (Cell Signaling Technology 5661, 1:1,000 for western blotting), total PKA (Cell Signaling Technology 4782, 1:1,000 for western blotting), Calcineurin B1 (Cell Signaling Technology 2614, 1:1,000 for western blotting), cleaved caspase-3 (Cell Signaling Technology 9661, 1:200 for immunofluorescence), p-Histone H3 (EMD Millipore 06-570, 1:500), Egr2 (1:1000 for immunohistochemistry) and Pou3f1 (1:100 for immunohistochemistry), both a generous gift from D. Mejier (University of Edinburgh). Chicken antibodies include antibodies to neurofilament M (Covance PKC-593P, 1:2,000 for immunohistochemistry), MPZ (Millipore AB9352, 1:500 for western blotting), GFP (Abcam 13970, 1:1,000 for immunohistochemistry). Rat MBP hybridoma (diluted 1:2 in immunohistochemistry) was a generous gift from V. Lee (University of Pennsylvania).

Secondary antibodies included DyLight 549 (Jackson ImmunoResearch 715-505-150, 1: 500 for immunohistochemistry), DyLight 488 (Jackson ImmunoResearch 703-485-155, 1:500 for immunohistochemistry), goat antibody to rabbit HRP (Jackson ImmunoResearch 111-035-003, 1:5.000 for western blotting). Infrared secondary antibodies for quantitative western blotting analyses were obtained from LI-COR Biosciences and all used 1:10,000 (goat antibody to mouse IRDye 680 926-68070; goat antibody to mouse IRDye 800 926-68070; goat antibody to rabbit IRDye 680 926-68021; goat antibody to rabbit IRDye 800 926-32211). Co-cultures were fixed in and permeabilized in 100% methanol at −20 °C for 15 min, stained and examined as described[31]. Sciatic nerves

were dissected from P2 mice and immediately fixed in 4% paraformaldehyde (vol/vol) in 0.1 M 1× PBS at +4 °C, cryo-protected in 20% sucrose (Sigma-Aldrich), embedded in OCT (Miles), and snap-frozen in liquid nitrogen. Sections were stained as described[58] and examined by epifluorescence on a Leica DM 4500 microscope and by confocal microscopy on a Leica SP5.

Statistical analyses. No statistical assays were used to pre-determine the sample size. Nonetheless, we chose samples of comparable size, especially to perform *in vitro* experiments. Data were collected randomly and assessed blindly. The data distribution was assumed to be normal, although we did not formally test it. Limma method used in the microarray differential expression analysis is based on an estimate of variance, which is moderated across genes[59]. All statistical analyses were performed on at least three different experiments. Statistical detailed analyses are reported in each figure legends and all assays (two sided Fischer's exact test, one-way ANOVA Dunnett's multiple comparison test, two sided moderate *t* test and two tailed unpaired *t* test) were performed using the Prism Software package (GraphPad).

A **Supplementary Methods Checklist** is available.

51. Eguchi, N. *et al.* Lack of tactile pain (allodynia) in lipocalin-type prostaglandin D synthase–deficient mice. *Proc. Natl. Acad. Sci. USA* **96**, 726–730 (1999).
52. Trivedi, S.G. *et al.* Essential role for hematopoietic prostaglandin D2 synthase in the control of delayed type hypersensitivity. *Proc. Natl. Acad. Sci. USA* **103**, 5179–5184 (2006).
53. Nelson, A.M. *et al.* Prostaglandin D2 inhibits wound-induced hair follicle neogenesis through the receptor, Gpr44. *J. Invest. Dermatol.* **133**, 881–889 (2013).
54. Quattrini, A. *et al.* Beta 4 integrin and other Schwann cell markers in axonal neuropathy. *Glia* **17**, 294–306 (1996).
55. Bolis, A. *et al.* Dlg1, Sec8 and Mtmr2 regulate membrane homeostasis in Schwann cell myelination. *J. Neurosci.* **29**, 8858–8870 (2009).
56. Wrabetz, L. *et al.* A minimal human MBP promoter-lacZ transgene is appropriately regulated in developing brain and after optic enucleation, but not in shiverer mutant mice. *J. Neurobiol.* **34**, 10–26 (1998).
57. Song, W.L., Lawson, J.A., Wang, M., Zou, H. & FitzGerald, G.A. Noninvasive assessment of the role of cyclooxygenases in cardiovascular health: a detailed HPLC/MS/MS method. *Methods Enzymol.* **433**, 51–72 (2007).
58. Pellegatta, M. *et al.* alpha6beta1 and alpha7beta1 integrins are required in Schwann cells to sort axons. *J. Neurosci.* **33**, 17995–18007 (2013).
59. Smyth, G. K. Linear models and empirical bayes methods for assessing differential expression in microarray experiments. *Stat. Appl. Genet. Mol. Biol.* **3**, 3 (2004).

Erratum: Prostaglandin D2 synthase/GPR44: a signaling axis in PNS myelination

Amelia Trimarco, Maria Grazia Forese, Valentina Alfieri, Alessandra Lucente, Paola Brambilla, Giorgia Dina, Damiana Pieragostino, Paolo Sacchetta, Yoshihiro Urade, Brigitte Boizet-Bonhoure, Filippo Martinelli Boneschi, Angelo Quattrini & Carla Taveggia
***Nat. Neurosci.*; doi:10.1038/nn.3857; corrected online 17 November 2014**

In the version of this article initially published online, a *P* value was incorrect on p. 5, first full paragraph. It read "We found similar alterations in 6-month-old sciatic nerves of *L-pgds*$^{-/-}$ mice, although the difference was not significant ($P = 0.649$; **Supplementary Table 2**)." The correct *P* value is 0.0649. Also, the first Results subheading read "NRG1 type III is cleaved and activates L-PGDS by γ-secretase"; it should have read "NRG1 type III is cleaved by γ-secretase and activates L-PGDS." The errors have been corrected for the print, PDF and HTML versions of this article.

Physical Medicine and Rehabilitation - International

Open Access

Austin Publishing Group

Case Report

Gait Training for Becker's Muscular Dystrophy Using Robot Suit Hybrid Assistive Limb

Asai T[1], Ojima I[1], Minami S[1], Takeshima Y[2] and Matsuo M[1,3]*

[1]Department of Physical Therapy, Kobegakuin University, Japan

[2]Department of Pediatrics, Hyogo College of Medicine, Japan

[3]Kobe University, Japan

*Corresponding author: Matsuo M, Department of Physical Therapy, Kobegakuin University, Japan, Tel: +81-78-974-2461; Fax: +81-78-974-2461; Email: mmatsuo@reha.kobegakuin.ac.jp

Received: October 03, 2014; **Accepted:** October 12, 2014; **Published:** October 14, 2014

Abstract

Becker's muscular dystrophy (BMD) is an X-linked recessive inherited disorder characterized by a slow and degenerative muscle weakness of the legs and pelvis. The patients eventually use walking aids or are wheelchair-bound in daily life because of the progression of disability. The robot suit hybrid assistive limb (HAL) is a new robot suit designed to assist voluntary control of lower limb motion by detecting extremely weak bioelectric signals on the skin surface. Here we report how HAL gait training can be adapted for a wheelchair-bound patient with BMD. A 25-year-old patient with BMD participated in HAL gait training.Gait training consisted of three phases: phase 1, adaptation of HAL for the patient; phase 2 (1 year), treadmill training with the body-weight supported walker (BWSW); and phase 3 (2 years), gait training on the floor with the BWSW. The subject completed 2 h of HAL gait training once a week (from August 2011 to August 2014). Although there are no standard exercises for patients with BMD, his gait ability and fitness improved, following HAL gait training. This result indicates that HAL gait training can be both feasible and safe when used as a part of a regular rehabilitation program for patients with BMD. Harness use seems to be essential for safety and feasibility of HAL gait for patients with BMD. The combined use of the HAL gait training and BWSW may be an effective rehabilitation tool for patients with BMD.

Keywords: Becker's muscular dystrophy; Hybrid assistive limb; Gait exercise; Body-weight supported walker

Introduction

Becker's muscular dystrophy (BMD) is an X-linked recessive inherited disorder, characterized by a slow and progressive degenerative muscle weakness of the legs and pelvis. Severity of the disease may markedly vary depending on the age of the patient at disease onset [1]. The patients eventually use walking aids or are wheelchair-bound in daily life because of progression of disability [2]. Rehabilitation exercises differ for ambulatory and wheelchair-bound patients. Gait training, activities of daily living (ADL) exercises and conventional physical therapy (stretching and range of motion at the lower limb joints) are practiced for ambulatory patients. Once patients become wheelchair-bound, gait training is no longer practiced; rehabilitation efforts instead focus on ADL exercises to maximize independent living.

The robot suit hybrid assistive limb (HAL) is a new robot suit designed to assist voluntary control of the knee and hip joint motion by detecting extremely weak bioelectric signals on the surface of the skin [3-5]. The HAL can support the wearer's lower limb motion while walking by adjusting the supportive level [3]. The HAL gait training is being increasingly employed for patients suffering from acquired neurological disease, such as stroke or spinal cord disease [4-9]. However, no studies have attempted to examine the feasibility of HAL rehabilitation for patients with BMD. Here we report a case in which the patient was wheelchair-bound and rehabilitation gait training had ceased. We report how HAL gait training can be adapted for use by a wheelchair-bound patient with BMD. Gait ability was influenced by HAL training.

Case Presentation

A 25-year-old patient with BMD (height, 164 cm; weight, 54 kg) participated in HAL gait training. He was diagnosed with BMD by dystrophin immune-staining of biopsied muscle tissue at 9 years of age because of the appearance of motor function deficits [10]. After the onset of BMD symptoms, his physical function gradually declined, and he began using a wheelchair outdoors at the age of 15. At the age of 22, walking was no longer possible. From the age of 23, he participated in conventional physical therapy, including muscle strength and range of motion exercises, twice a week in preparation for HAL gait training. At the age of 25, he started HAL gait training in addition to conventional physical therapy. Prior to participating in HAL gait training, the subject provided informed consent; the study was approved by the Ethics Committee of the Kobegakuin University (HEB121211-1).

Mode Setting of HAL

The HAL has a hybrid control system consisting of Cybernic Voluntary Control (CVC) and Cybernic Autonomous Control (CAC) [9]. The CVC supports the patient's voluntary lower limb motion according to the voluntary muscle activity and assistive torque provided to each joint. In this study, we used the CVC, which allows the operator to adjust the degree of physical support to the patient's comfort. In addition, the HAL has two modes, walking mode and stand up mode, which support voluntary movement of walking and standing up, respectively, according to the electrical signals of muscle contracture and load on the feet. In this study, we used the walking

Citation: Asai T, Ojima I, Minami S, Takeshima Y and Matsuo M. Gait Training for Becker's Muscular Dystrophy Using Robot Suit Hybrid Assistive Limb. Phys Med Rehabil Int. 2014;1(3): 4.

Table 1: Summary of gait training.

Phase 1 Adaptation of HAL suit for patient	Phase 2 (1 year) Treadmill training with BWSW	Phase 3 (2 years) Gait training on the floor with BWSW
• Search for the body parts to detect the bioelectrical signal for hip extension. • Apply the special harness to BWSW.	• 2 h of training once a week (gait training: 1 h). • The treadmill speed was adjusted to patient's condition (0.6–1.6 km/h) • The gait speed of the treadmill and the walking distance during training increased (the distance that the patient walked before the heart rate reached 125 bpm).	• 2 h of training once a week (gait training: 1 h) • Walking speed was adjusted by a therapist to pull the BWSW but not exceeding the heart rate of 125 bpm. • Walking distance during training increased (the distance that the patient walked before the heart rate reached 125 bpm). • 5 times sit-to-stand exercise after gait training

mode for gait training and stand up mode for sit-to-stand exercises. Furthermore, we monitored the heart rate during gait training to ensure that the working load was safe and appropriate.

Training

Gait training consisted of three phases: phase 1, adaptation of HAL for the patient; phase 2, treadmill training with the body-weight supported walker (BWSW); and phase 3, gait training on the floor with the BWSW. Typical gait training (phases 1 and 2) proceeded as follows: attaching electrodes, wearing the HAL and harness, and setting up the computer (45 min); HAL gait training (60 min, including rest time); removing the HAL and harness (15min). In phase 3, five sit-to-stand exercises (5STS) were added after gait training. All gait trainings and 5 STS were conducted by three physical therapists. The training phase is summarized in Table 1.

Phase 1: Adaptation of HAL suit for the patient

According to the manufacturer's instructions, electrodes for the hip extension were attached just below the ischial tuberosity. However, sufficient electrical signals of muscle contraction were not detected in this area. Several electrodes were placed on different sites around the hip joints, and an area on the upper part of the gluteus maximus muscle was found to enable bioelectrical signal detection (Figure 1). When applying the HAL, we used BWSW to adjust the working load (Figure 2). BWSW is a modified body support system, which has been used for the HAL gait training for patients with stroke and spinal cord injury [9, 11]. A HAL supplier-recommended special harness in the BWSW was used for the patient (Figure 3A). We were able to adjust the height of patient from the floor using a handle on the outside of the frame (Figure 3B). In addition, this system can be set up to be used with a treadmill or as a special walker on the floor (Figure 4, 5).

Phase 2: Treadmill training with BWSW

In this phase, the subject under went 2 h of HAL gait training once a week for 1 year (Figure 4). The treadmill speed was adjusted to the patient's condition. The subject could not continue walking with HAL so much after his heart rate reached at 125 bpm. For the safety reason, 125 bpm was set as the discontinuance criteria for the HAL gait training. The treadmill speed and walking distance during the training was the speed and distance before his heart rate reached at 125 bpm, and they were gradually increased (Figure 6). We started with a treadmill speed of 0.6 km/hr and walking distance of 200 meters, because he felt the difficulty of walking with HAL in the begining and his heart rate reached at 125 bpm very easily. Near the end of phase 2, the subject could walk at a speed of 1.6 km/h and walk a distance of >700 meters. Additionally, the subject walked on the treadmill with 1-3° incline in the last 100 meters when his condition was good. His average heart rate was approximately 110 bpm during walking.

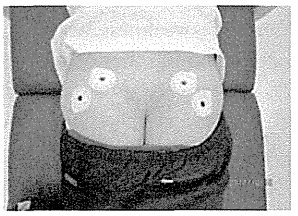

Figure 1: Locations of electrodes for hip extension.

Figure 2: Body-weight supported walker.

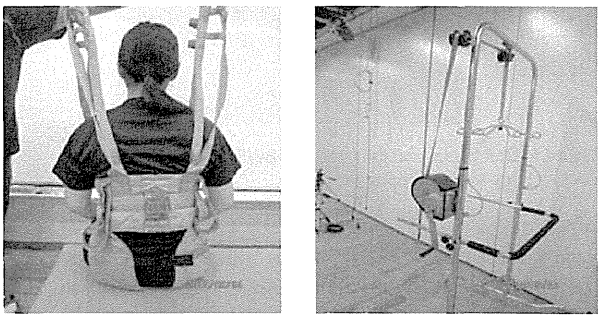

A: The harness for gait training

B: Handle for the adjustment of patient height

Figure 3: Treadmill training with the BWSW with harness.
BWSW: body-weight supported walker
A: The harness for gait training,
B: Handle for the adjustment of patient height

Phase 3: Gait training on the floor using the BWSW

After phase 2, we began gait training on the floor (Figure 5).

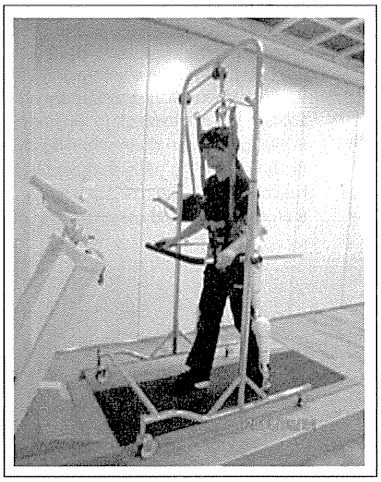

Figure 4: Treadmill training with BWSW.
BWSW: body-weight supported walker.

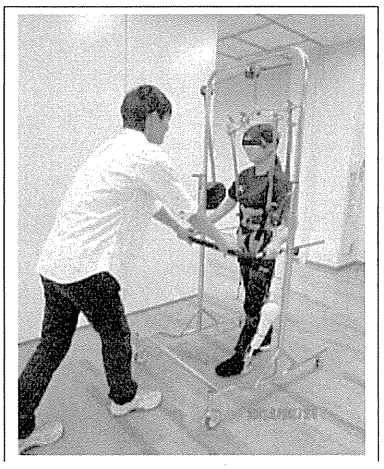

Figure 5: Gait training on the floor with BWSW.
BWSW: body-weight supported walker.

Walking speed was adjusted by a therapist to pull the BWSW but not exceed a heart rate of 125 bpm. The initial walking distance during training was less than 200 meters, but it was gradually increased to approximately 500 meters (Figure 6). After gait training and some rest, 5STS was performed. Three therapists helped the subject stand up on a platform, which was 50 cm above the floor. One therapist was in front to manually support him stand up, and the other two assisted from the sides to pull up the harness. His heart rate frequently reached 125 bpm during the last 5STS trial. When his heart rate reached 125 bpm before the last trial, we stopped the exercise immediately. Clinical assessments were performed at the initial evaluation and 3 years after HAL gait training (Table 2).

Discussion

This case report describes the feasibility of HAL gait training for patients with BMD. In general, patients with neuromuscular disease do not undergo gait training during the non-ambulatory phase [12]. This patient had not undergone gait training since he had become wheelchair-bound. Although there are no standard exercises for patients with BMD or severe Duchenne muscular dystrophy [13], his

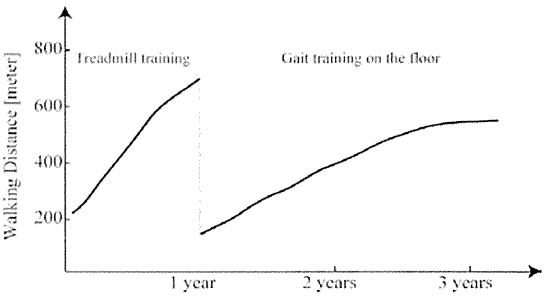

Figure 6: The time course of walking distance during gait training.
Walking distance: The distance that the patient walked during training before his heart rate reached 125 bpm.

Table 2: Results of clinical assessments.
BMI, body mass index; ROM, range of motion; R/L, Right/Left; MMT, manual-muscle testing.

	Pre-training (initial evaluation)	Post-training (3 years later)
Body weight (kg)	56	54
BMI	20.8	20.1
ROM (°)		
Hip extension (R/L)	−30/−20	−25/−20
Knee extension (R/L)	−20/−15	−20/−15
Ankle dorsiflexion(R/L)	−25/−25	−25/−20
MMT		
Hip extension (R/L)	2−/2−	2−/2−
Knee extension (R/L)	2−/2−	2−/2−
Shoulder flexion (R/L)	2/2	2/2
Shoulder extension (R/L)	2/2	2/2
Elbow extension (R/L)	3/3	3/3
Brook upper extremity scale	2	2
Vignos lower extremity scale	9	9

gait ability and fitness improved with HAL gait training. This finding indicates that HAL gait training is both feasible and safe when used as a part of a regular rehabilitation program for patients with BMD.

All gait trainings were performed using BWSW, which provided safety and gait speed control. The combined use of the HAL and BWSW is important for HAL gait training in patients with BMD. The combination allowed the patient to stop walking whenever he wanted. Although the BWSW height occasionally limited the reduction of weight load, it was satisfactory in the present case. The use of a harness seems essential to allow safe HAL gait training for patients with BMD.

The HAL training began long after the patient became wheelchair-bound. HAL gait training at an early phase may be necessary to prevent lower limb muscle weakness or joint contracture due to disuse syndrome as described in other conditions [9]. In the present case, the training frequency was relatively limited (once a week, Table 1). Furthermore, other physical exercises, such as knee extension exercise with HAL, were not performed. Other physical functions, such as muscle strength and range of motion, may be recovered by additional HAL trainings. Finally, improvement was not observed in the clinical assessment (Table 2). Other medication should be

combined with HAL gait training to achieve clinical improvement. Further study is needed in this area.

Conclusion

For patients with BMD, HAL gait training may be an effective rehabilitation tool.

Acknowledgment

The authors would like to thank Enago (www.enago.jp) for the English language review.

References

1. Emery AE, Skinner R . Clinical studies in benign (Becker type) X-linked muscular dystrophy. Clin Genet. 1976; 10: 189-201.
2. Emery AE . The muscular dystrophies. Lancet. 2002; 359: 687-695.
3. Kawamoto H, Sankai Y: Power assist method based on Phase Sequence and muscle force condition for HAL.Adv Robot2005, 19: 717-734.
4. Maeshima S, Osawa A, Nishio D, Hirano Y, Takeda K, Kigawa H,et al . Efficacy of a hybrid assistive limb in post-stroke hemiplegic patients: a preliminary report. BMC Neurol. 2011; 11: 116.
5. Sakakima H, Ijiri K, Matsuda F, Tominaga H, Biwa T, Yone K, et al: A newly developed robot suit hybrid assistive limb facilitated walking rehabilitation after spinal surgery for thoracic ossification of the posterior longitudinal ligament: a case report.Case Rep Orthop 2013, 2013: 621405.
6. Kubota S, Nakata Y, Eguchi K, Kawamoto H, Kamibayashi K, Sakane M, et al . Feasibility of rehabilitation training with a newly developed wearable robot for patients with limited mobility. Arch Phys Med Rehabil. 2013; 94: 1080-1087.
7. Kawamoto H, Kamibayashi K, Nakata Y, Yamawaki K, Ariyasu R, Sankai Y, et al . Pilot study of locomotion improvement using hybrid assistive limb in chronic stroke patients. BMC Neurol. 2013; 13: 141.
8. Ueba T, Hamada O, Ogata T, Inoue T, Shiota E, Sankai Y . Feasibility and safety of acute phase rehabilitation after stroke using the hybrid assistive limb robot suit. Neurol Med Chir (Tokyo). 2013; 53: 287-290.
9. Nilsson A, Vreede KS, Häglund V, Kawamoto H, Sankai Y, Borg J . Gait training early after stroke with a new exoskeleton - the hybrid assistive limb: a study of safety and feasibility. J Neuroeng Rehabil. 2014; 11: 92.
10. Takeshima Y, Yagi M, Okizuka Y, Awano H, Zhang Z, Yamauchi Y, et al: Mutation spectrum of the dystrophin gene in 442 Duchenne/Becker muscular dystrophy cases from one Japanese referral center.J Hum Genet 2010, 55: 379-388.
11. Aach M, Cruciger O2, Sczesny-Kaiser M3, Höffken O3, Meindl RC2, Tegenthoff M3, et al . Voluntary driven exoskeleton as a new tool for rehabilitation in chronic spinal cord injury: a pilot study. Spine J. 2014; .
12. Bushby K, Finkel R, Birnkrant DJ, Case LE, Clemens PR, Cripe L, et al . Diagnosis and management of Duchenne muscular dystrophy, part 1: diagnosis, and pharmacological and psychosocial management. Lancet Neurol. 2010; 9: 77-93.
13. Bushby K, Finkel R, Birnkrant DJ, Case LE, Clemens PR, Cripe L, et al . Diagnosis and management of Duchenne muscular dystrophy, part 2: implementation of multidisciplinary care. Lancet Neurol. 2010; 9: 177-189.

Citation: Asai T, Ojima I, Minami S, Takeshima Y and Matsuo M. Gait Training for Becker's Muscular Dystrophy Using Robot Suit Hybrid Assistive Limb. Phys Med Rehabil Int. 2014;1(3): 4.

Journal of Bioscience and Bioengineering
VOL. 118 No. 1, 116–118, 2014

ELSEVIER

www.elsevier.com/locate/jbiosc

TECHNICAL NOTE

Practical evaluation of liquid chromatography/tandem mass spectrometry and enzyme immunoassay method for the accurate quantitative analysis of prostaglandins

Yoshihiro Izumi,[1] Kosuke Aritake,[2] Yoshihiro Urade,[2] and Eiichiro Fukusaki[1,*]

Department of Biotechnology, Graduate School of Engineering, Osaka University, 2–1 Yamadaoka, Suita, Osaka 565-0871, Japan[1] and Department of Molecular Behavioral Biology, Osaka Bioscience Institute, 6-2-4 Furuedai, Suita, Osaka 565-0874, Japan[2]

Received 15 November 2013; accepted 24 December 2013
Available online 16 February 2014

The accurate and robust measurement of prostaglandins (PG) concentration could help to understand the many physiological functions. The present study revealed that liquid chromatography/tandem mass spectrometry method for the PGs analysis can satisfy the requirements for both qualitative and quantitative performance as compared to competitive enzyme immunoassays.

[**Key words:** Prostaglandins; Liquid chromatography/tandem mass spectrometry; Enzyme immunoassay; Quantitative accuracy; Immunological cross-reaction]

Prostaglandins (PG) are lipid mediators derived from arachidonic acid that regulate many physiological and pathophysiological functions. PGD_2 and PGE_2, both of which are positional isomers produced by cyclooxygenases (COX1 and COX2), are representative prostanoids. PGE_2 is a potent stimulant and functions in inflammation, gastric and intestinal secretion, regulation of blood pressure, platelet aggregation, and so on (1). PGD_2, which is secreted by mast cells, Th2 cells, and dendritic cells, has long been implicated in allergic inflammation (2). In addition, PGD_2 is well known as one of the most potent sleep-inducing substances in the central nervous system of mammals (3,4). Since important biological events such as inflammation, mediating pain, and fever are indeed finely modulated by the levels of PGD_2 and PGE_2 at low concentration, the analyses of these metabolites require a highly sensitive and accurate quantitative methodology.

Bioassay methods such as competitive enzyme immunoassay (EIA) are the most commonly used quantitative procedure for the measurement of individual PG due to their sensitivity and specificity, which is a consequence of the unique ligand-antibody binding (4). However, the antibody preparation required for this technique is rather laborious, and cross-reactivity of the antibody with other compounds including prostaglandin analogs may be inevitable. Meanwhile, mass spectrometry-based techniques, especially liquid chromatography/tandem mass spectrometry (LC/MS/MS) under multiple-reaction monitoring (MRM), have attracted attention in the quantification of PGs owing to their selectivity (5,6). To date, no previous evaluation of EIA and LC/MS/MS method for the PGD_2 and PGE_2 analyses in terms of sensitivity and quantitative accuracy has been reported. The accurate measurement of PGs concentration could help to understand the underlying mechanisms and possibility of therapeutic interventions.

The aim of the present study is to examine the applicability of two commercially available EIAs to the measurement of PGD_2 and PGE_2, both of which are secreted by rat mast cells stimulated with dinitrophenyl-BSA, along with comparison to an LC/MS/MS assay (Fig. 1).

Rat mast cell line (RBL-2H3 cells) was purchased from the Health Science Research Resources Bank (HSRRB, Osaka, Japan). RBL-2H3 cells were cultured in Minimum Essential Medium (MEM, Sigma–Aldrich Co., St. Louis, MO, USA) containing 10% heat-inactivated fetal bovine serum, 100 units mL^{-1} penicillin, and 100 μg mL^{-1} streptomycin sulfate. After the sensitization of RBL-2H3 cells with 50 ng mL^{-1} monoclonal anti-dinitrophenyl IgE, the cells were stimulated with 20 ng mL^{-1} dinitrophenyl-BSA, and culture medium was picked up at 1, 3, 5, 10, and 15 min after the stimulation. Cultured medium was purified with Sep-Pak C18 Plus cartridge with 360 mg sorbent (Waters Corp., Miliford, MA, USA). Briefly, medium samples were diluted with ethanol (final ethanol concentration of 15% v/v) containing the radioisotope labeled standards of $[^3H_7]PGE_2$ and $[^3H_7]PGD_2$ (60 Bq for each per assay) (Perkin-Elmer Inc., Boston, MA, USA) for EIA as tracers for estimation of the recovery, or the stable isotope labeled standards of $[^2H_4]PGE_2$ and $[^2H_4]PGD_2$ (10 pmol) (Cayman Chemical Co., Ann Arbor, MI, USA) for LC/MS/MS analysis with the standard isotope-dilution method. The cartridges were conditioned with 10 mL of ethanol and allowed to equilibrate with 10 mL of Milli-Q water. Each sample was loaded on a cartridge, and then the cartridge was washed with 20 mL of hexane. The PGs-mixture was eluted with 5 mL of ethyl acetate to glass tube. The eluates were dried by evaporation under a stream of dry nitrogen. For the quantitative analysis of PGD_2 and PGE_2 with LC/MS/MS, the dried sample was reconstituted in 100 μL of water/methanol/acetic acid (90/10/0.05, v/v/v).

* Corresponding author. Tel./fax: +81 6 6879 7424.
E-mail address: fukusaki@bio.eng.osaka-u.ac.jp (E. Fukusaki).

1389-1723/$ – see front matter
http://dx.doi.org/10.1016/j.jbiosc.2013.12.022

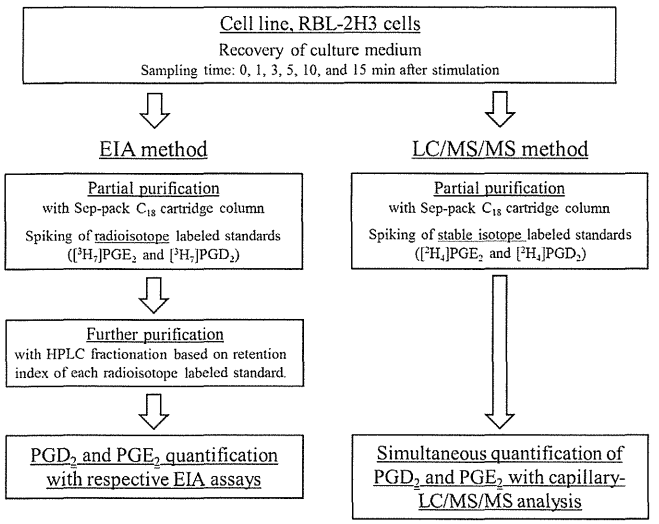

FIG. 1. Overview of EIA and LC/MS/MS protocols for the determination of PGD_2 and PGE_2.

In the case of EIA, the further purification of PGs was performed by HPLC fractionation (7). Finally, the quantification of PGD_2 and PGE_2 was performed with respective EIA kits (Cayman Chemical Co.) according to the methods describing in the instructions. LC/MS/MS system was composed of an LC Packings Ultimate equipped with a Switchos loading pump and a Famos autosampler (Dionex Corp., Sunnyvale, CA, USA) and an Esquire 3000 plus ion-trap mass spectrometer fitted with an ESI ion source (Bruker Daltonics Inc., Billerica, MA, USA). The LC/MS/MS analysis was performed under the following conditions: trapping column, Inertsil ODS-3 C18 column (0.3 × 5 mm, particle size of 5 μm, Dionex Corp.); mobile phase for sample loading, 0.05% (v/v) acetic acid in water; flow rate for sample loading, 10 μL min^{-1}; separation column, Inertsil ODS-3 C18 column (0.3 × 150 mm, particle size of 3 μm, GL Sciences Inc., Tokyo, Japan); sample loading time, 5 min; mobile phase for PGs separation, water/acetonitrile/acetic acid (95/5/0.05, v/v/v) (A) and acetonitrile/water/acetic acid (95/5/0.05, v/v/v) (B); flow rate: 4 μL min^{-1}; gradient curve, 40% B at 0 min, 50% B at 15 min, 90% B at 17 min, 90% B at 22 min, 40% B at 23 min, and 40% B at 30 min; injection volume, 10 μL; mode of mass analysis, negative ion mode; nebulizer flow, 9.0 psi; dry gas flow rate of 4.0 L min^{-1}; dry gas temperature, 250°C; capillary voltage, 4.5 kV; compound stability, 100%, trap drive level, 50%; target count, 10,000; maximum accumulation time, 100 ms; and spectral average, 7. The MS/MS spectra were analyzed in the auto MS/MS mode at fragmentation amplitude of 1.0 V. MRM transitions from the precursor ions to the most abundant product-ions were recorded. The optimized MRM transitions are as follows: PGD_2 and PGE_2, 350.8 > 314.8; and [$^2H_4$]PGD_2 (d_4-PGD_2) and [$^2H_4$]PGE_2 (d_4-PGE_2), 354.8 > 318.8.

The present study has evaluated the analytical capabilities (i.e., sensitivity, quantitative accuracy, and sample throughput) between LC/MS/MS and EIAs method based on the practical protocols for the PGs quantification (Fig. 1). EIAs assay is a very useful tool for the individual PG analysis in terms of economical, high throughput performance, and highly sensitive. However, EIAs may not provide specificity sufficient for the determination of PGs if immunological cross-reactions occur, since the antibodies used in EIA sometimes recognize not only the target molecule, but also structurally related molecules. Therefore, in our practical EIA protocol, after the partial purification of PGs with Sep-pack C_{18} cartridge, the further purification of each targeted PG was performed using HPLC fractionation based on retention index of each corresponding radioisotope labeled standard (7). On the other hand, in the LC/MS/MS analysis, the PGD_2 and PGE_2 were quantified by a standard isotope-dilution. The standard isotope-dilution method refers to the addition of the stable isotopomers of the target compounds prior to partial purification, enables the accurate quantification by compensating for both losses due to the sample pretreatment step and the nonspecific matrix effects caused by co-eluting components (8). In addition, it is well known that the sensitivity of LC/MS/MS can be increased by lowering the flow rate of the mobile phase, which can be achieved by using narrow diameter LC columns (9). Thus, we selected to the capillary LC system for PGs analysis.

The detection sensitivity of the LC/MS/MS system developed in this study was compared to commercially available EIA kits with PGD_2 and PGE_2 standard solutions. The limits of detection (LOD) of LC/MS/MS was estimated based on $S/N = 3$ in the LC/MS/MS separation, whereas the LOD of EIAs was calculated with 80% B/B_0 (% bound/maximum bound: ratio of the absorbance of a particular sample or standard well to that of the maximum binding B_0 well) value. The detection limits of LC/MS/MS were 1.5 nM (PGD_2) and 0.70 nM (PGE_2), while the LODs of EIAs were 0.15 nM (PGD_2) and 0.10 nM (PGE_2). Thus, the sensitivity of EIA was approximately 10-fold higher than that of LC/MS/MS, indicating that EIA measurement will lead to a minimization of starting material than the LC/MS/MS system used.

Fig. 2A shows the LC/MS/MS (MRM) chromatograms of deuterium-labeled internal standards and PGs released from RBL-2H3 cells stimulated with dinitrophenyl-BSA. The LC/MS/MS assay was able to separate the PGD_2, PGE_2, and unidentified metabolite (PGX) and detect them with same MRM transition. Next, the performance of quantitative accuracy of LC/MS/MS and EIAs was compared (Fig. 3). Based on the statistical analysis, the LC/MS/MS method for PGD_2 has no significant fault and can produce results compatible with EIA measurement (Fig. 3B). However, significant difference in the quantification of PGE_2 was observed between the LC/MS/MS and EIA strategies (Fig. 3A). The level of PGE_2 estimated using EIA was 3–8 times higher than that estimated with LC/MS/MS.

Here, in order to investigate the cause of analytical error of quantitative values between the two methodologies, we focused on the peak of the PGX, which represents the same MRM transition as PGD_2 and PGE_2 but different elution time (Figs. 2A and 3C). By means of product-ion scan mode in the ion-trap mass spectrometer, the MS/MS spectra of the PGE_2, PGD_2, and PGX were acquired by equal collision-induced dissociation parameter (Fig. 2B–D). The dissociation pattern of PGX was very similar to that of PGD_2 and PGE_2 (especially PGD_2). Previous study has revealed that a series of PG-like compounds termed isoprostanes are formed *in vivo* from the free radical-catalyzed peroxidation of arachidonate independent of COX (10). In addition, Brose et al. reported previously that the optimized LC/MS/MS method allows for the PGs (PGD_2 and PGE_2) and their stereoisomers, namely isoprostanes including entPGE_2, 8-isoPGE_2, 11β-PGE_2, and 15(R)-PGD_2 to be separated (6). Therefore, this unidentified peak, PGX is probably attributed to the stereoisomer of PGD_2 or PGE_2, or their mixtures. Considering our present findings and previous reports, the quantitative values of PGE_2 with EIA protocol will contain a part of PGX (Fig. 3C). Conceivably, PGE_2 fraction would be contaminated with PGX in the process of HPLC fractionation based on retention index of [$^3H_7$]PGE_2. Furthermore, antibody used in immunoassay for PGE_2 would recognize not only the PGE_2, but also structurally related molecule, PGX. Thus, these results raise the possibility that PGs might be overestimated by EIA compared with LC/MS/MS method, especially in a trace amount of metabolite such as PGE_2 in the present case.

Taking all of the present results into account, LC/MS/MS method is suitable than EIAs for PGs analysis in terms of quantitative accuracy, which would be useful for the underlying mechanisms of biological functions including sleep, central nervous system injury,

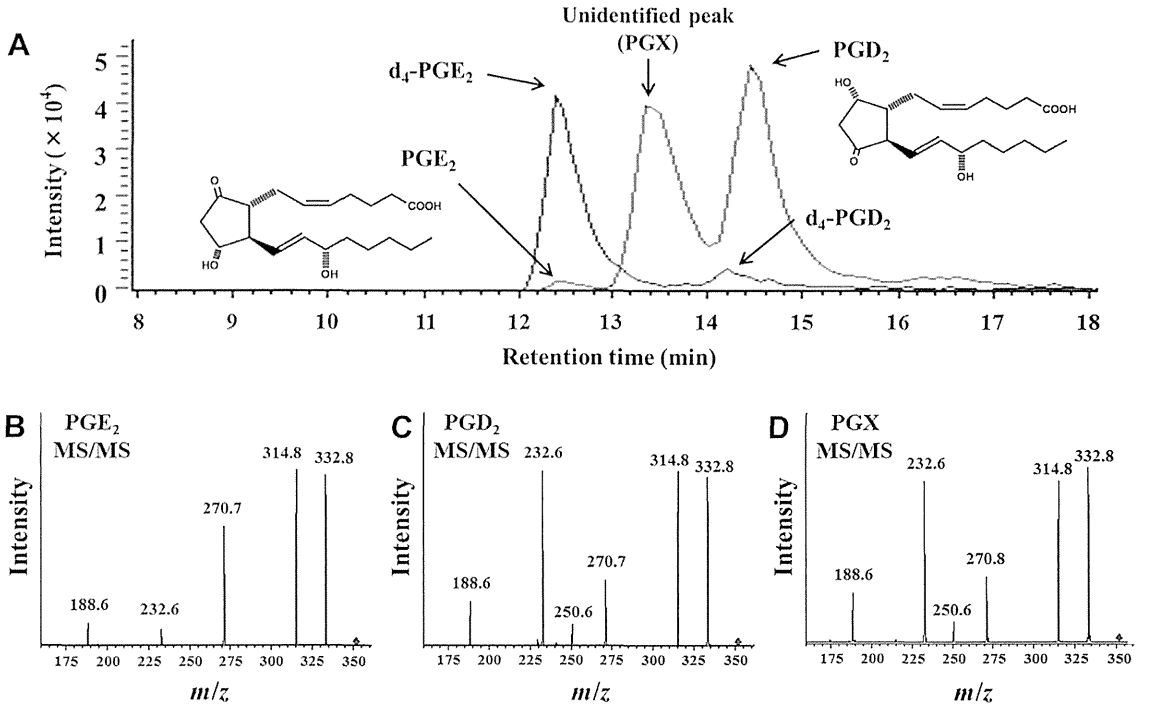

FIG. 2. LC/MS/MS (MRM) chromatograms of PGs released from RBL-2H3 cells with dinitrophenyl-BSA stimulation (A). Fragmentation patterns of PGE_2 (B), PGD_2 (C), and unidentified PGX (D) by means of product-ion scan.

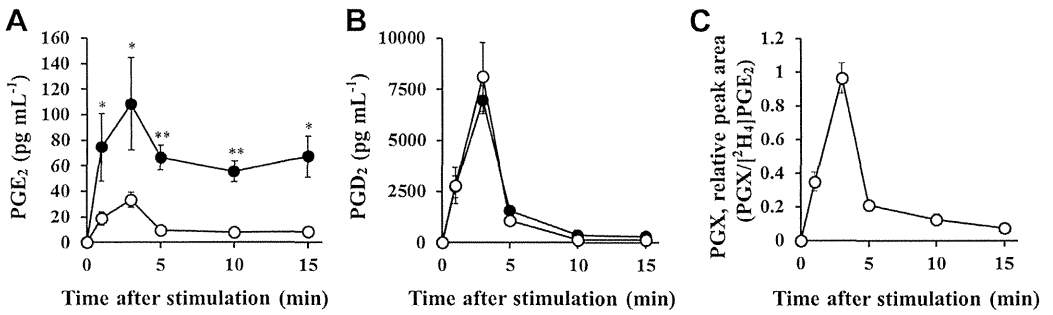

FIG. 3. Quantitative estimation of time-dependent production of PGE_2 (A), PGD_2 (B), and PGX (relative peak area) (C) in RBL-2H3 cells using LC/MS/MS (open circles) and EIA (closed circles). Error bars indicate standard deviations of five biological replicates. Equality of variances of each data point between LC/MS/MS and EIA results was judged by *F*-test at the 99% confidence level ($P > 0.01$, Student's *t*-test; $P < 0.01$, Welch's *t*-test). Statistical significance was then determined using Student's or Welch's *t*-test ($^*P < 0.01$, $^{**}P < 0.001$).

inflammation, and cancer, as well as the possibility of therapeutic treatments. In addition, more recently, the improvement of an LC/MS/MS analytical system enables the comprehensive and quantitative analysis of PGs and their related metabolites with high throughput (11). Accordingly, we predict that LC/MS/MS approach will be widely used as a standard method for the precise, robust, and simultaneous profiling of PGs.

References

1. **Kalinski, P.:** Regulation of immune responses by prostaglandin E_2. J. Immunol., **188**, 21–28 (2012).
2. **Arima, M. and Fukuda, T.:** Prostaglandin D_2 and T_H2 inflammation in the pathogenesis of bronchial asthma. Korean J. Intern. Med., **26**, 8–18 (2011).
3. **Hayaishi, O.:** Molecular mechanisms of sleep-wake regulation: roles of prostaglandins D_2 and E_2. FASEB J., **11**, 2575–2581 (1991).
4. **Pinzar, E., Kanaoka, Y., Inui, T., Eguchi, N., Urade, Y., and Hayaishi, O.:** Prostaglandin D synthase gene is involved in the regulation of non-rapid eye movement sleep. Proc. Natl. Acad. Sci. USA, **97**, 4903–4907 (2000).
5. **Schmidt, R., Coste, O., and Geisslinger, G.:** LC–MS/MS-analysis of prostaglandin E_2 and D_2 in microdialysis samples of rats. J. Chromatogr. B, **826**, 188–197 (2005).
6. **Brose, S. A., Thuen, B. T., and Golovko, M. Y.:** LC/MS/MS method for analysis of E_2 series prostaglandins and isoprostanes. J. Lipid Res., **52**, 850–859 (2011).
7. **Pandey, H. P., Ram, A., Matsumura, H., and Hayaishi, O.:** Concentration of prostaglandin D_2 in cerebrospinal fluid exhibits a circadian alteration in conscious rats. Biochem. Mol. Biol. Int., **37**, 431–437 (1995).
8. **Liu, R. H., Lin, D. L., Chang, W. T., Liu, C., Tsay, W. I., Li, J. H., and Kuo, T. L.:** Isotopically labeled analogues for drug quantitation. Anal. Chem., **74**, 618A–626A (2002).
9. **Izumi, Y., Okazawa, A., Bamba, T., Kobayashi, A., and Fukusaki, E.:** Development of a method for comprehensive and quantitative analysis of plant hormones by highly sensitive nanoflow liquid chromatography–electrospray ionization-ion trap mass spectrometry. Anal. Chim. Acta, **648**, 215–225 (2009).
10. **Gao, L., Zackert, W. E., Hasford, J. J., Danekis, M. E., Milne, G. L., Remmert, C., Reese, J., Yin, H., Tai, H.-H., Dey, S. K., Porter, N. A., and Morrow, J. D.:** Formation of prostaglandins E_2 and D_2 via the isoprostane pathway. J. Biol. Chem., **278**, 28479–28489 (2003).
11. **Blaho, V. A., Buczynski, M. W., Brown, C. R., and Dennis, E. A.:** Lipidomic analysis of dynamic eicosanoid responses during the induction and resolution of Lyme arthritis. J. Biol. Chem., **284**, 21599–21612 (2009).

Opposing Immunomodulatory Roles of Prostaglandin D_2 during the Progression of Skin Inflammation

Hana Sarashina,* Yoshiki Tsubosaka,† Keisuke Omori,* Kosuke Aritake,‡ Takayuki Nakagawa,§ Masatoshi Hori,* Hiroyuki Hirai,¶ Masataka Nakamura,‖ Shuh Narumiya,# Yoshihiro Urade,‡ Hiroshi Ozaki,* and Takahisa Murata†

The effects of PGD_2 are extremely context dependent. It can have pro- or anti-inflammatory effects in clinically important pathological conditions. A greater mechanistic insight into the determinants of PGD_2 activity during inflammation is thus required. In this study, we investigated the role of PGD_2 in croton oil–induced dermatitis using transgenic (TG) mice overexpressing hematopoietic PGD synthase. Administration of croton oil caused tissue swelling and vascular leakage in the mouse ear. Compared with wild-type animals, TG mice produced more PGD_2 and showed decreased inflammation in the early phase, but more severe manifestations during the late phase. Data obtained from bone marrow transplantation between wild-type and TG mice indicated that PGD_2 produced by tissue resident cells in the TG mice attenuated early-phase inflammation, whereas PGD_2 produced from hematopoietic lineage cells exacerbated late-phase inflammation. There are two distinct PGD_2 receptors: D-prostanoid receptor (DP) and chemoattractant receptor–homologous molecule expressed on Th2 cells (CRTH2). In TG mice, treatment with a DP antagonist exacerbated inflammation in the early phase, whereas treatment with a CRTH2 antagonist attenuated inflammation during the late phase. In vitro experiments showed that DP agonism enhanced vascular endothelial barrier formation, whereas CRTH2 agonism stimulated neutrophil migration. Collectively, these results show that when hematopoietic PGD synthase is overexpressed, tissue resident cell–derived PGD_2 suppresses skin inflammation via DP in the early phase, but hematopoietic lineage cell–derived PGD_2 stimulates CRTH2 and promotes inflammation during the late phase. DP-mediated vascular barrier enhancement or CRTH2-mediated neutrophil activation may be responsible for these effects. Thus, PGD_2 represents opposite roles in inflammation, depending on the disease phase in vivo. ***The Journal of Immunology*****, 2014, 192: 459–465.**

Prostaglandins are metabolites of arachidonic acid generated by cyclooxygenase (COX) that are synthesized and released upon encountering injurious stimuli. COX-mediated PG synthesis is generally categorized as a proinflammatory event. For instance, a major PG, PGE_2, triggers common inflammatory symptoms, including swelling, pain, and fever (1, 2). Another prostanoid, TXA_2, promotes platelet aggregation and vascular contraction (3). Clinically, inhibition of COX-mediated PG synthesis has been applied to treat several types of inflammatory diseases, including arthritis (4) and colorectal cancer (5).

PGD_2 is reported to promote sleep and to mediate inflammatory responses. PGD synthase is of two types: lipocalin-type PGD synthase and hematopoietic PGD synthase (H-PGDS). Lipocalin-type PGD synthase is expressed mainly in the arachnoid and choroid membrane, and is implicated in sleep (6) and pain promotion (7). In contrast, H-PGDS is expressed mainly in immune cells, such as mast cells and Th2 lymphocytes, and contributes to various inflammatory responses in peripheral tissues (8). PGD_2 exerts its effects via two types of receptors: D-prostanoid receptor (DP) and chemoattractant receptor–homologous molecule expressed on Th2 cells (CRTH2). The half-life of PGD_2 in blood is short (0.9 min) (9). Several in vitro and in vivo studies have shown that PGD_2 is quickly degraded to several products through enzymatic and/or nonenzymatic pathways (10, 11), and that these products also stimulate PGD_2-dependent pathways. Whereas PGD_2 and its degradation product, PGJ_2, can bind DP and CRTH2 equally, many of the other products, such as $9\alpha,11\beta$-PGF_2, 13,14-dihydro-15-keto-PGD_2 (DK-PGD_2), and 15-deoxy-$\Delta^{12,14}$-PGD_2 (15d-PGD2), possess higher binding affinity for CRTH2 (12–14). J-ring PGs also exhibit bioactivity, as they are ligands for the peroxisome proliferator–activated receptor-γ (15–17). Although the pathophysiological implications of each PGD_2 metabolite in vivo remain elusive, various activities have been ascribed to these degradation products.

Reports have proved contradictory regarding whether PGD_2 is pro- or anti-inflammatory. For instance, administration of PGD_2 or a DP agonist has anti-inflammatory effects in rat bowel inflammation (18)

*Department of Veterinary Pharmacology, Graduate School of Agriculture and Life Sciences, The University of Tokyo, Tokyo 113-8657, Japan; †Department of Animal Radiology, Graduate School of Agriculture and Life Sciences, The University of Tokyo, Tokyo 113-8657, Japan; ‡Department of Molecular Behavioral Biology, Osaka Bioscience Institute, Osaka 565-0874, Japan; §Department of Veterinary Surgery, Graduate School of Agriculture and Life Sciences, The University of Tokyo, Tokyo 113-8657, Japan; ¶Advanced Medicine and Development, BML, Inc., Saitama 350-1101, Japan; ‖Human Gene Sciences Center, Tokyo Medical and Dental University, Tokyo 113-8150, Japan; and #Department of Pharmacology, Faculty of Medicine, Kyoto University, Kyoto 606-8315, Japan

Received for publication August 7, 2013. Accepted for publication November 1, 2013.

This work was supported by the Program for Promotion of Basic and Applied Researches for Innovations in Bio-oriented Industry (Grant 12100979); the Ministry of Education, Culture, Sports, Science and Technology and the Japan Society for the Promotion of Science (Grants 22688024 and 25252049); the Mochida Memorial Foundation; and the Towa Foundation (to T.M.).

Address correspondence and reprint requests to Prof. Takahisa Murata, Department of Animal Radiology, Graduate School of Agriculture and Life Sciences, University of Tokyo, 1-1-1 Yayoi, Bunkyo-ku, Tokyo 113-8657, Japan. E-mail address: amurata@mail.ecc.u-tokyo.ac.jp

The online version of this article contains supplemental material.

Abbreviations used in this article: BAEC, bovine aortic endothelial cell; BM, bone marrow; BMT, bone marrow transplantation; COX, cyclooxygenase; CRTH2, chemoattractant receptor–homologous molecule expressed on Th2 cell; $CRTH2^{-/-}$, CRTH2 deficient; DK-PGD_2, 13,14-dihydro-15-keto-PGD_2; DP, D-prostanoid receptor; $DP^{-/-}$, DP deficient; H-PGDS, hematopoietic PGD synthase; TER, transendothelial electric resistance; TG, transgenic; VEGF, vascular endothelial growth factor; WT, wild-type.

www.jimmunol.org/cgi/doi/10.4049/jimmunol.1302080

and mouse atopic dermatitis (19). DP receptor agonism inhibited eosinophil migration (20) and dendritic cell activation (21) in a mouse model of asthma. Our group also proved that PGD_2 suppressed mouse acute lung inflammation and tumor growth by inhibiting vascular permeability and subsequent angiogenesis via DP stimulation (22, 23). According to these observations, the PGD_2-DP axis is likely to exert anti-inflammatory effects. In contrast, several other groups showed that PGD_2 signaling mediates proinflammatory responses. For example, administration of an H-PGDS inhibitor improved mouse airway inflammation (24). Furthermore, treatment with a CRTH2 agonist aggravated atopic dermatitis and asthma in mice, whereas intratracheal administration of PGD_2 promoted eosinophil migration in rats (25, 26). Thus, PGD_2 is likely to regulate inflammation differently, depending on the disease type.

The overall outcome of an inflammatory response is determined by multiple factors, including the type of mediator-producing cell/effector cell, the precise effector cell function, the amount of inflammatory signal produced, and the identity of the receptor receiving the stimulus. Furthermore, these factors vary according to the site and phase of inflammation. Because PGD_2 and its metabolites exert various actions through several signal pathways, detailed studies investigating where and how PGD_2 is produced, and its effects in discrete phases of discrete diseases, are indispensable for the design of future therapies.

In the current study, we compared inflammatory reactions in the skin between transgenic (TG) mice overexpressing H-PGDS and wild-type (WT) mice to evaluate the contribution of PGD_2 at each stage of disease progression. We demonstrate that PGD_2-DP signaling originating in tissue resident cells alleviates vascular permeability in the early phase of croton oil–induced dermatitis, and that PGD_2-CRTH2 signaling in infiltrating hematopoietic cells promotes inflammation during the late phase of dermatitis.

Materials and Methods

Reagents

Croton oil, vascular endothelial growth factor (VEGF), and Evans blue were from Sigma-Aldrich; Triton X-100, paraformaldehyde, formamide, and methyl acetate were from Wako Pure Chemical; PGD_2, BW 245C, BW A868C, CAY10471, AL 8810, SQ29548, 15-deoxy-$\Delta^{12,14}$-PGD_2, 9α,11β-PGF_2, DK-PGD_2, anti–H-PGDS Ab, and anti–COX-2 Ab were from Cayman Chemical; anti-CD45 Ab was from Millipore; and penicillin-streptomycin was from Life Technologies.

Mouse dermatitis model

All animal experiments were performed in accordance with the guidelines of the University of Tokyo. TG mice with FVB background expressing human H-PGDS under the regulatory control of the chicken β-actin promoter were generated as previously described (27). Among the three lines of TG mice (S41, S55, and S66), S55 was used, as they exhibited the most abundant mRNA expression and enzymatic activity of human H-PGDS. DP deficient ($DP^{-/-}$) and CRTH2 deficient ($CRTH2^{-/-}$) mice with C57BL/6 background were generated and bred as described previously (28, 29). In some experiments, bone marrow transplantation (BMT) was performed as previously described (22). Recipient mice (4–5 wk old) were irradiated with 4.5 Gy, twice with 12-h intervals. Bone marrow (BM) cells (2×10^5) were collected from femurs of donor mice (8–9 wk old) and injected through the tail vein of the recipient. Mice were used for each experiment 8 wk after BMT. Mice were anesthetized with isoflurane. Croton oil (2.5%, 2 h or 6 h) was administered to the surface of the right ear of mice. VEGF (30 ng per head, 35 min), 9α,11β-PGF_2 (10 ng per head each, 40 min), or DK-PGD_2 (10 ng per head each, 40 min) was injected s.c. into the right ear. Vehicle was administered to the left ear as an internal control.

Modified Miles assay

After a certain period from the time of administration of each reagent to the ears, mice were i.v. injected with Evans blue (30 mg/kg for FVB TG mice or 50 mg/kg for C57BL/6 gene–deficient mice). At 30 min after the circulation, the ears were dissected and dried overnight at 55°C. After the ears were weighed, Evans blue was extracted by incubation in formamide at 55°C for 24 h. Dye content was measured by reading at 610 nm in a spectrophotometer (Wallac 1420, PerkinElmer) and normalized to ear dry weight.

Measurement of PGs

Contents of PGD_2, PGE_2, and TXA_2 in ears were measured as previously described (30). Briefly, excised ears were quickly frozen into liquid nitrogen and homogenized in ethanol containing 0.02% HCl, and the samples were separated by HPLC. An API3200 triple-quadruple tandem mass spectrometer (Applied Biosystems) was used.

Immunostaining

Ear tissues were fixed in 4% paraformaldehyde for 2 d and embedded in paraffin. Sections of 4-μm thickness were stained with H&E. For immunostaining, 5-μm-thick frozen sections were used. After permeabilization/blocking with 0.1% Triton X-100 and 5% normal goat serum for 30 min, sections were labeled with anti–H-PGDS Ab (1:400), anti–COX-2 Ab (1:250), or anti-CD45 Ab (1:400) overnight at 4°C. Then, the sections were labeled with secondary Ab and DAPI. The images were captured using an Eclipse E800 fluorescence microscope (Nikon), and the number of $CD45^+$ cells was counted in three randomly chosen fields in each slide.

Measurement of transendothelial electric resistance

Bovine thoracic aortas were purchased from a slaughterhouse. Bovine aortic endothelial cells (BAECs) were isolated and cultured in DMEM containing 10% FBS. BAECs (2.5×10^4) were seeded into each well of the microelectronic sensor, and then transendothelial electric resistance (TER) was measured by xCELLigence real time cell analyzer DP system (Roche). Confluent monolayers of BAECs were serum starved for 10 h before the experiment. TER was measured every 30 s and then normalized to the initial value.

Isolation of neutrophil and chemotaxis assay

Marrow cavities of the tibias and femurs of 8-wk-old mice were flushed with DMEM. Neutrophils were isolated by centrifugation over discontinuous Percoll gradients. For the chemotaxis assay, a modified Boyden chamber

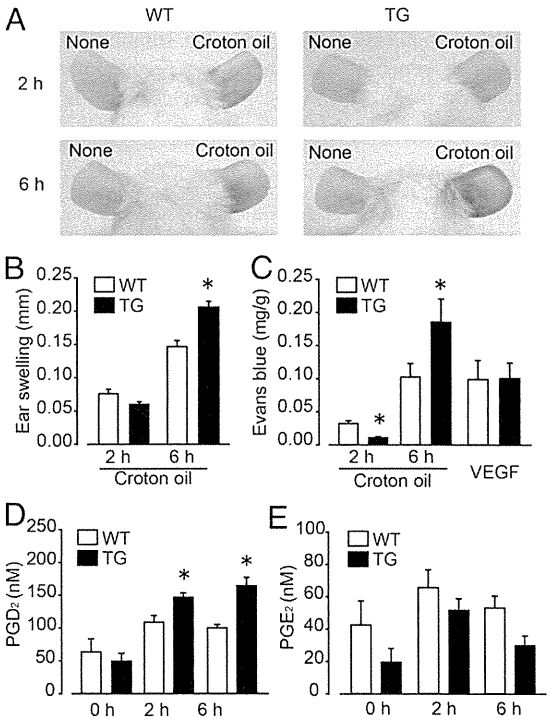

FIGURE 1. Croton oil–induced skin inflammation in H-PGDS–overexpressing mice. Croton oil (2.5%, 2 h or 6 h) or VEGF (30 ng, 35 min) was administered to mouse ears. Evans blue dye (30 mg/kg) was injected and circulated for 30 min. (**A**) Representative photographs show croton oil–induced inflammation. Skin thickness (**B**) or dye extravasation (**C**) of the inflamed ears was quantified (n = 5–8 each, $*p < 0.05$ compared with WT). The concentration of PGD_2 (**D**) or PGE_2 (**E**) in inflamed ears was determined by a mass spectrometer (n = 5, $*p < 0.05$ compared with WT).

with 8-μm pores (BD Falcon) was used. Stimulants were added to the bottom chamber, and inhibitors were added to both the upper and the bottom chambers. Isolated neutrophils (2×10^5 cells) were applied to the upper chambers. After 2 h, cells on the membrane were fixed and stained with Giemsa solution. The number of cells from five randomly chosen fields (×200) on the lower side of the membrane was counted.

Data representation and statistical analysis

The results are expressed as mean ± SEM. Statistical evaluations of the data were performed using an unpaired Student *t* test for comparisons between two groups and by one-way ANOVA followed by a Dunnett test or Tukey test for comparison between more than two groups. A $p < 0.05$ was taken as significant.

Results

Inflammatory responses in the presence of H-PGDS overexpression

In WT mice, administration of 2.5% croton oil caused ear swelling (Fig. 1B) and increased dye extravasation, an index of vascular permeability (typical pictures are shown in Fig. 1A, and dye leakages are quantified in Fig. 1C). These responses peaked 6 h after the stimulation and settled in 36 h (ear swelling, 6 h, 0.146 ± 0.013 mm; 36 h, 0.012 ± 0.005 mm, $n = 5$ each).

Pretreatment with a pan-COX inhibitor, indomethacin, inhibited these responses (Supplemental Fig. 1), suggesting the contributions of PG production to the inflammation. TG mice showed reduced severity of ear swelling and less vascular leakage at the early phase (2 h after the stimulation), but showed more severe inflammation than WT mice at the late phase (6 h post treatment). WT and TG mice responded similarly to treatment with VEGF, which directly stimulates vascular leakage without activation of the arachidonate cascade (Fig. 1C, *right bars*).

Administration of 2.5% croton oil induced PGD_2 production in both WT and TG mice (Fig. 1D). PGD_2 production in TGs, compared with that in WT mice, was significantly higher during the experiments. The concentration of another prostanoid, PGE_2, did not differ between the lines (Fig. 1E).

Infiltrated leukocytes expressed H-PGDS

As shown by the H&E staining (Fig. 2A, *upper panels*), no morphological difference was observed between WT and TG mice prior to stimulation (0 h). There was a time-dependent ear swelling and infiltration of inflammatory cells upon croton oil administration. Most of the infiltrating cells were neutrophils with segmented nuclei (Fig. 2A, *middle and lower panels*; see insets). Regarding the ear-swelling data shown in Fig. 1B, TG ears were slightly thinner at the early phase of inflammation, whereas they were much thicker than WT ears at the late phase. Neutrophil infiltration was also accelerated in TG mice at the late phase (Fig. 2A, inset panels).

We next performed immunostaining to define which type of cell expresses H-PGDS in inflamed ears. As shown in Fig. 2B (*upper left panels*), H-PGDS was not detected in nontreated WT ears. In croton oil–treated WT ears, $CD45^+$ leukocytes expressed H-PGDS (Fig. 2B, *middle and lower left panels*). TG ears broadly expressed H-PGDS regardless of oil stimulation (Fig. 2B, *left panels*). These observations are consistent with the fact that human H-PGDS is constitutively expressed in the TG mice from a chicken β-actin promoter. Of interest, oil stimulation increased H-PGDS expression even in TG mice, and in particular in the $CD45^+$ cells. This finding may be due to the elevation of endogenous mouse H-PGDS expression in response to stimulation.

Expression of an inducible type of COX, COX-2, is required to produce PGD_2 in the context of inflammation. As shown in Sup-

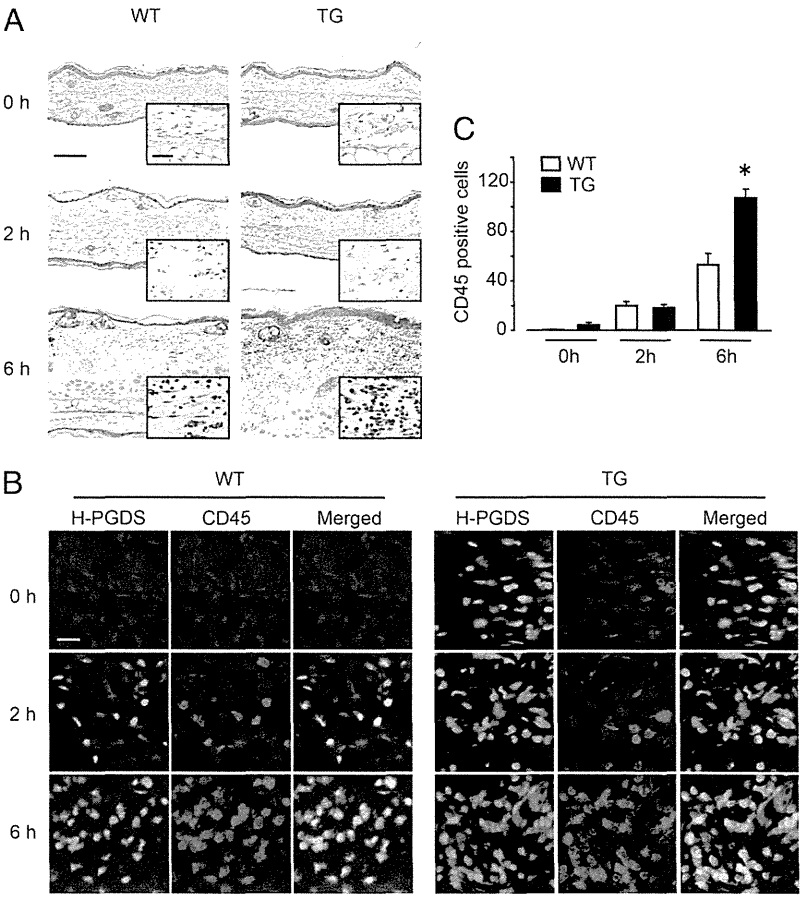

FIGURE 2. Infiltrating leukocytes expressed H-PGDS in inflamed ears. (**A**) Representative images of H&E stainingare shown. (**B**) Excised ears from WT or TG mice were subjected to immunostaining for H-PGDS (green) and CD45 (red), and then stained with DAPI (blue) for nuclear labeling ($n = 4$ each). The pictures were randomly taken from three fields, each at a magnification of ×200 from four dependent sections. Scale bar, 20 μm. (**C**) The number of $CD45^+$ cells was counted ($n = 4$, $^*p < 0.05$ compared with WT).

plemental Fig. 2A and 2B, $CD31^+$ vascular endothelial cells constitutively express COX-2 in both lines of mice. Infiltrating $CD45^+$ leukocytes (most likely neutrophils) also express COX-2 after stimulation. We thus inferred that these two cell types are the major sources of PGD_2 in this model.

In agreement with the observations from H&E staining, a significant difference was noted in the number of infiltrating leukocytes between the lines during the early phase of inflammation. In contrast, many more leukocytes infiltrated TG ears than WT ears at the late phase (Fig. 2C).

Functional contribution of hematopoietic lineage–derived PGD_2 in dermatitis

We explored the contribution of hematopoietic cell (BM-derived immune cells)– or nonhematopoietic cell (tissue resident cells)–derived PGD_2 in dermatitis using BMT. Irradiated WT recipients with WT BM (WT + WT^{BM}) exhibited tissue swelling comparable to that in nontreated WT (Supplemental Fig. 3) in response to oil treatment. The BMT procedures (i.e., radiation and BM injection) did not affect the inflammatory responses. At the early phase of inflammation (2 h), no difference was detected in ear swelling between the lines (Fig. 3A), whereas TG transplanted with WT or TG BM (TG + WT^{BM} and TG + TG^{BM}) exhibited blunted vascular leakage compared with WT with WT or TG BM (WT + WT^{BM} and WT + TG^{BM}) (Fig. 3B). These results suggest that PGD_2 secreted from the tissue resident cells inhibits the inflammation in TG mice during the early phase of dermatitis.

At the late phase, regardless of recipient genotype, mice transplanted with TG BM (WT + TG^{BM}, TG + TG^{BM}) showed more severe swelling (Fig. 3C) and vascular leakage (Fig. 3D) in comparison with the mice with WT BM (WT + WT^{BM}, TG + WT^{BM}). This finding indicates that PGD_2 from infiltrating hematopoietic cells (most presumably neutrophils) promotes inflammatory responses in the TG during this phase.

The role of PGD_2-DP signaling in the early phase of inflammation

We attempted to clarify how PGD_2 modulated inflammatory responses during early-phase dermatitis. Administration of an H-PGDS inhibitor, HQL-79 (50 mg/kg, i.p.), significantly enhanced tissue swelling (Fig. 4A) and vascular permeability (Fig. 4B) in both lines of mice. Upon H-PGDS inhibition, the degrees of ear swelling and dye extravasation were similar in WT and TG mice. As with H-PGDS inhibition, DP antagonism by BW A868C (1 mg/kg, i.p.) also promoted inflammatory responses in both WT and TG mice to the same degree (Fig. 4C, 4D).

Thus, the DP-mediated signal most likely contributed to the immunosuppressive reaction of PGD_2 in early-phase inflammation. In support of this idea, $DP^{-/-}$ mice were more responsive to croton oil stimulation than were WT mice, whereas $CRTH2^{-/-}$ mice exhibited responses comparable to those of WT mice. Additive treatment with PGD_2 (1 mg/kg, i.p.) inhibited the oil-induced vascular leakage in WT and $CRTH2^{-/-}$ mice, but not $DP^{-/-}$ mice (Fig. 4E). Furthermore, administration of a DP agonist, BW 245C (1 mg/kg, i.p.), strongly inhibited vascular leakage in WT ears (Fig. 4F).

The role of PGD_2-CRTH2 signaling in late-phase inflammation

We next assessed the contribution of PGD_2 to late-phase dermatitis. As shown in Fig. 5A and 5B (ear swelling and dye leakage, respectively), inhibition of H-PGDS by HQL-79 (50 mg/kg, i.p.) tended to increase the scores in WT mice, whereas it attenuated them in TG mice. As shown in Fig. 5C and 5D (both data are shown

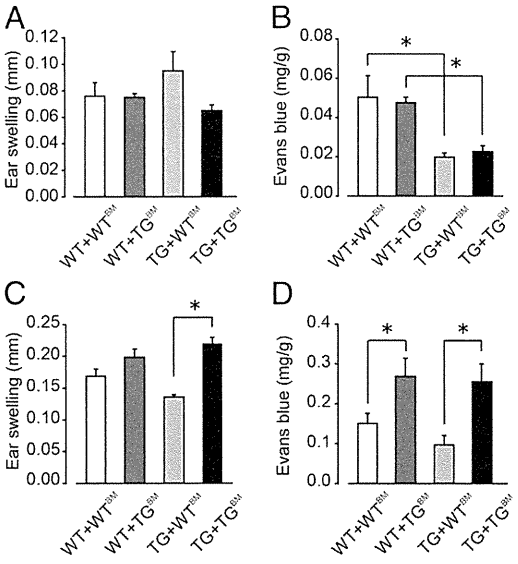

FIGURE 3. Contribution of hematopoietic lineage–derived PGD_2 in dermatitis. Ear swelling (thickness) and dye extravasation in each BMT mouse were assessed 2 h (**A** and **B**) or 6 h (**C** and **D**) after croton oil treatment (n = 5 or 6 each, $^*p < 0.05$).

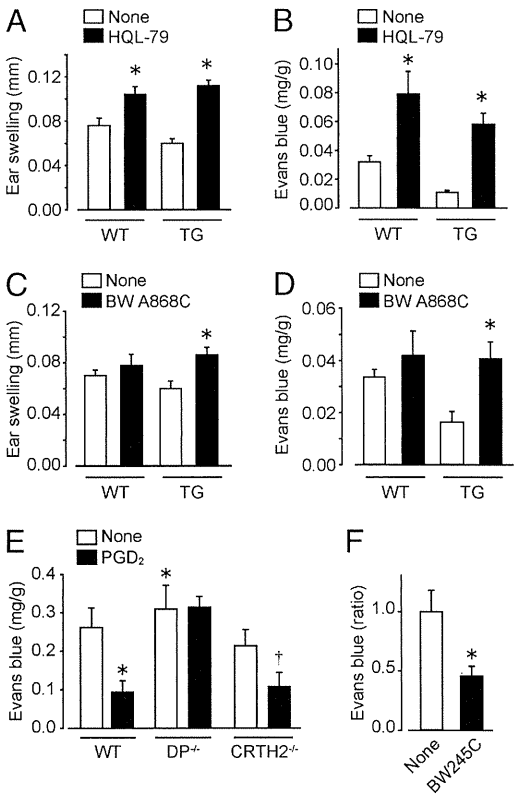

FIGURE 4. DP signaling alleviated early-phase inflammation. Effects of an H-PGDS inhibitor, HQL-79 (50 mg/kg, i.p., 3 h before the stimulation), or a DP antagonist, BW A868C (1 mg/kg, i.p., 2 h before the stimulation), on the ear swelling (**A** and **C**) and tissue dye extravasation (**B** and **D**) were assessed. Dye extravasation during early-phase inflammation were assessed in $DP^{-/-}$ or $CRTH2^{-/-}$ mice with C57BL/6 background (**E**). PGD_2 (1 mg/kg, i.p.) was administered 10 min before the stimulation. Effect of a DP agonist, BW 245C (1 mg/kg, i.p., 10 min before dye injection), on dye efflux during early-phase inflammation was assessed (**F**). The data are indicated as a ratio to nontreated ears (only with croton oil administration) (n = 4–6, $^*p < 0.05$ and $^\dagger p < 0.05$, compared with nontreated WT ears or $CRTH2^{-/-}$ ears).

as a ratio to nontreated), DP antagonism (BW A868C, 1 mg/kg i.p.) promoted, and CRTH2 antagonism (CAY10471, 1 mg/kg, i.p.) tended to attenuate, the oil-induced inflammation in both lines of mice. The DP-mediated anti-inflammatory reaction was dominant in WT mice, whereas the CRTH2-mediated proinflammatory signal appeared to counteract DP-mediated responses in TG mice.

We could obtain consistent observations using gene-deficient mice. As shown in Fig. 5E, WT and CRTH2$^{-/-}$ mice represented comparable vascular leakage responding to sole oil treatment (6 h). DP deficiency significantly increased vascular leakage even in late-phase dermatitis. Additional treatment with PGD_2 increased vascular permeability in WT and increased slightly, but not significantly, in DP$^{-/-}$ mice. In contrast, PGD_2 treatment significantly decreased vascular permeability in CRTH2$^{-/-}$ mice.

As described above, PGD_2 is rapidly degraded into several products in blood (10, 11). These products possibly accumulate locally and preferentially stimulate CRTH2-mediated proinflammatory signaling according to disease progression. Indeed, treatment with the major PGD_2 metabolites DK-PGD_2 and 9α,11β-PGF_2 (10 ng per ear) significantly enhanced vascular leakage (Fig. 5F).

The effect of PGD_2 on vascular permeability and neutrophil migration in vitro

We examined the effect of PGD_2 on vascular endothelial permeability by measuring TER in vitro. In line with the in vivo data showing DP-mediated vascular barrier enhancement (Fig. 4E), treatment with PGD_2 (10 μM) or BW 245C (1 μM) elevated TER, indicating barrier enhancement (typical responses are shown in Fig. 6A and summarized in Fig. 6B). These effects were completely inhibited by DP antagonism (BW A868C, 10 μM, 30 min before PGD_2 administration). A CRTH2 agonist, DK-PGD_2 (1 μM), which enhanced vascular permeability in vivo, did not change TER in vitro. In addition, 9α,11β-PGF_2 (1 μM) did not affect endothelial barrier formation in vitro (Fig. 6B).

In the transmembrane migration assay, isolated neutrophils migrated toward a solution of 5 nM leukotriene B_4 added into the lower chamber (Fig. 6C), as previously reported (31). Stimulation with PGD_2 or a DK-PGD_2 (1 μM), 9α,11β-PGF_2 (100 nM), also induced neutrophil migration; this was abolished by CRTH2 antagonism (CAY10471, 1 μM).

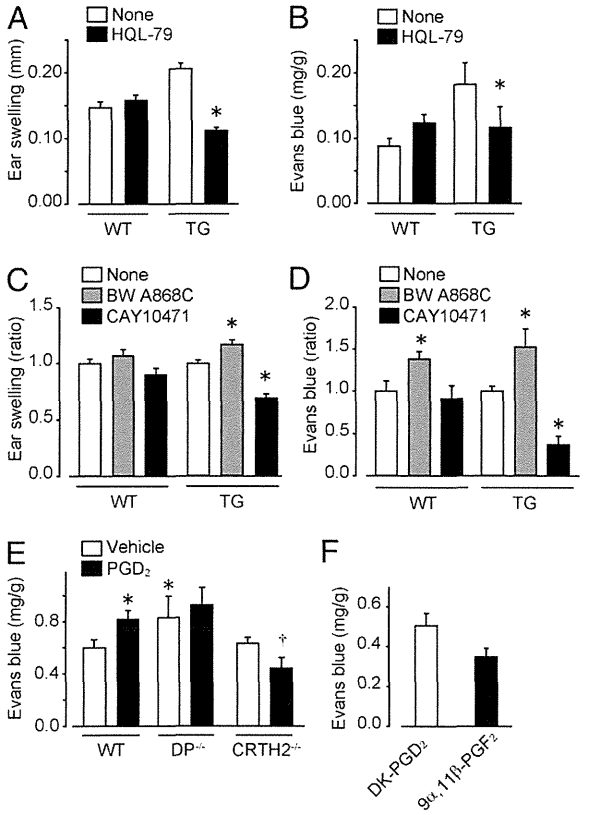

FIGURE 5. CRTH2 signaling promotes late-phase inflammation. Effects of HQL-79 [50 mg/kg, i.p., 3 h before the oil treatment (**A**)] or a DP antagonist, BW A868C [1 mg/kg, i.p., 2 h before the oil treatment (**B**)], or a CRTH2 antagonist, CAY10471 [1 mg/kg, i.p., 30 min before the oil treatment (B) on the late-phase ear swelling (A and **C**) and dye extravasation (B and **D**)]. Dye extravasation during late-phase inflammation was assessed in DP$^{-/-}$ or CRTH2$^{-/-}$ mice with C57BL/6 background (**E**). PGD_2 (1 mg/kg, i.p.) was administered 10 min before the stimulation. Effect of a CRTH2 agonist, DK-PGD_2 (10 ng per ear), or a PGD_2 metabolite, 9α,11β-PGF_2 (10 ng per ear), on vascular permeability in vivo (**F**) (n = 4–9 each, $^*p < 0.05$ compared with nontreated WT ears or CRTH2$^{-/-}$ ears).

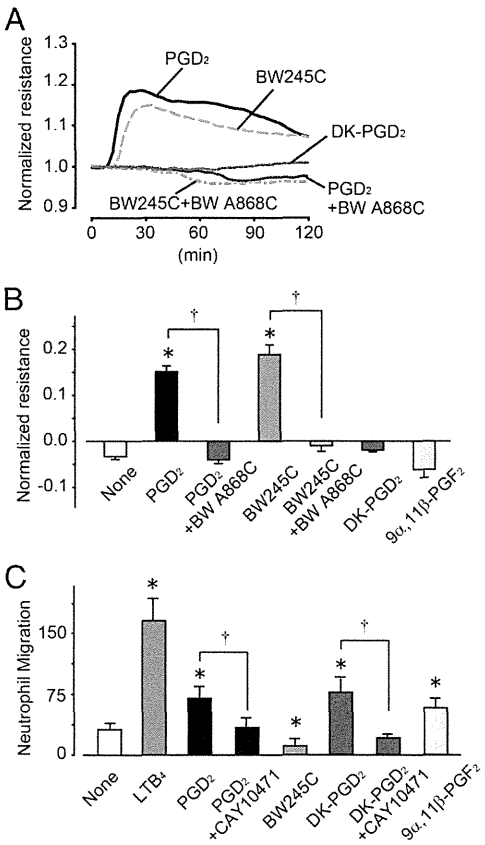

FIGURE 6. The effect of PGD_2 on vascular endothelial barrier formation and neutrophil migration. A representative figure (**A**) or quantification (**B**) of the TER is shown (n = 4–6 each, $^*p < 0.05$ and $^\dagger p < 0.05$ compared with nontreated or stimulant-treated cells). BAECs were treated with PGD_2 (10 μM), BW 245C (1 μM), DK-PGD_2 (1 μM), or 9α,11β-PGF_2 (1 μM). BW A868C (10 μM) was given 30 min before the PGD_2 or BW 245C treatment. Migration assay was performed using isolated neutrophils (**C**). Stimulants were added to the lower chamber, and CAY10471 (1 μM) was added to both the lower and the upper chambers. Data are shown as the number of cells migrating to the lower chamber in one field (×20, n = 5 each, $^*p < 0.05$ and $^\dagger p < 0.05$ compared with nontreated or stimulant-treated cells).

Discussion

Using genetically modified mice that overexpress H-PGDS, we demonstrated that PGD_2 assumes both pro- and anti-inflammatory roles according to the progression of inflammation. Specifically, upon initiation of croton oil–induced dermatitis, PGD_2 produced from tissue resident cells exhibits an anti-inflammatory action through DP-mediated signaling. At the progression phase, PGD_2, and possibly its degradation products secreted from infiltrating leukocytes, promote inflammation through CRTH2-mediated signaling (Supplemental Fig. 4).

At the early phase of dermatitis, secreted PGD_2 had anti-inflammatory activity in both WT and TG mice, which is attributable to DP-mediated signaling. TG showed relatively strong anti-inflammatory reactions. These phenomena are presumably due to the higher level of PGD_2 production in TG ears. The experiments using BMT revealed that PGD_2 produced from tissue resident cells contributes to the anti-inflammatory reaction during the early phase. Given that vascular endothelial cells constitutively express COX-2 (which is indispensable for PGD_2 production), endothelial cell–derived PGD_2 is likely to control inflammation in early-phase dermatitis.

We observed that DP-mediated signaling contributes to the anti-inflammatory role of PGD_2 by enhancing endothelial barrier formation. We previously reported that vascular endothelial cells express DP and its agonism inhibits vascular leakage in the inflamed lung (22) and growing tumor (23), in agreement with our current observations. The underlying molecular mechanism associated with stimulation of DP is tightening of endothelial cell-to-cell junctions through the cAMP/protein kinase A/Rac signaling pathway (32).

Of interest, in contrast to its anti-inflammatory role in the early phase, secreted PGD_2 showed proinflammatory effects in the late phase. When compared with the ears of WT animals, the ears of TG mice had more severe inflammation with increased PGD_2 production. BMT and morphological studies suggested that infiltrating leukocytes produced PGD_2 and promoted tissue swelling and vascular hyperpermeability. Considering the fact that tissue contents of PGD_2 were similar in the early and late phases in each line of mice (Fig. 1D), the site of production seems to be more crucial than the amount of PGD_2 for PGD_2-mediated immune responses.

We further demonstrated that CRTH2 signaling mediates the proinflammatory effects of PGD_2. This activity is likely because many of the PGD_2 degradation products potentially bind CRTH2 (12). Further investigation is required to assess the contribution of each product to the pathogenesis of inflammation, especially in vivo. However, it is possible that sustained local inflammation leads to the accumulation of PGD_2 metabolites, which further accelerate inflammation by acting as CRTH2 ligands.

Our data show that both a CRTH2 agonist (DK-PGD_2) and a major PGD_2 metabolite (9α,11β-PGF_2) enhanced vascular permeability in vivo, but they did not directly influence endothelial barrier formation in vitro. Previous studies showed that CRTH2 stimulation promotes the migration of BM-derived hematopoietic lineage cells such as Th2 lymphocytes and eosinophils (33). Consistently, CRTH2 agonism stimulated migration of neutrophils in vitro. In addition, infiltration of neutrophils was accelerated in inflamed TG ears. Neutrophils produce a variety of bioactive agents, including cytokines and reactive oxygen, that can stimulate the vascular bed (34). Thus, neutrophil-derived PGD_2 may promote neutrophil infiltration/migration through CRTH2 signaling, and as a result, bioactive substances released from infiltrating neutrophils could promote inflammation, at least partially, by disrupting the vascular barrier.

Our data showing that the PGD_2–DP signaling axis mediates anti-inflammatory reactions imply that DP agonism may be a strategy for treatment of various inflammatory diseases. Conversely, we also showed in this article that activation of the PGD_2–CRTH2 signal axis in inflammatory cells promotes inflammation. These situations presumably occur in diseases that are accompanied by local accumulation of PGD_2-secreting immune cells, such as allergic inflammation with mast cell and/or eosinophil accumulation. H-PGDS inhibition or CRTH2 antagonism might be beneficial for these pathological conditions.

Inflammation is an indispensable response for the rejection of foreign substances and for tissue regeneration, and it occurs throughout the body. As key players in this response, PGs are likely produced and received by almost all types of cells. To understand and manage various types of inflammatory diseases, a detailed evaluation of the role of individual PG types with respect to their source and effects in each phase of disease is an absolute requirement. We suggest that our use of the H-PGDS TG mice that overexpress H-PGDS with a β-actin promoter provides significant insight in this regard. The system is not without caveats, however, because the inflammatory symptoms observed in the TG mice were induced owing to exogenous expression of H-PGDS driven by a nonnative promoter. However, this mouse model highlighted the role of PGD_2 in inflammation and allowed us to provide deep insights into the paradoxical action of PGD_2.

In summary, the Janus-like behavior of PGD_2 with regard to its pro- and anti-inflammatory effects in vivo was determined by an exquisite balance of multiple factors, which included the site of its production and the quantity of PGD_2 and related degradation products.

Disclosures

The authors have no financial conflicts of interest.

References

1. Stock, J. L., K. Shinjo, J. Burkhardt, M. Roach, K. Taniguchi, T. Ishikawa, H. S. Kim, P. J. Flannery, T. M. Coffman, J. D. McNeish, and L. P. Audoly. 2001. The prostaglandin E2 EP1 receptor mediates pain perception and regulates blood pressure. *J. Clin. Invest.* 107: 325–331.
2. Ushikubi, F., E. Segi, Y. Sugimoto, T. Murata, T. Matsuoka, T. Kobayashi, H. Hizaki, K. Tuboi, M. Katsuyama, A. Ichikawa, et al. 1998. Impaired febrile response in mice lacking the prostaglandin E receptor subtype EP3. *Nature* 395: 281–284.
3. Furci, L., D. J. Fitzgerald, and G. A. Fitzgerald. 1991. Heterogeneity of prostaglandin H2/thromboxane A2 receptors: distinct subtypes mediate vascular smooth muscle contraction and platelet aggregation. *J. Pharmacol. Exp. Ther.* 258: 74–81.
4. Bingham, C. O., III 2002. Development and clinical application of COX-2-selective inhibitors for the treatment of osteoarthritis and rheumatoid arthritis. *Cleve. Clin. J. Med.* 69(Suppl 1): SI5–SI12.
5. Gupta, R. A., and R. N. Dubois. 2001. Colorectal cancer prevention and treatment by inhibition of cyclooxygenase-2. *Nat. Rev. Cancer* 1: 11–21.
6. Qu, W. M., Z. L. Huang, X. H. Xu, K. Aritake, N. Eguchi, F. Nambu, S. Narumiya, Y. Urade, and O. Hayaishi. 2006. Lipocalin-type prostaglandin D synthase produces prostaglandin D2 involved in regulation of physiological sleep. *Proc. Natl. Acad. Sci. USA* 103: 17949–17954.
7. Eguchi, N., T. Minami, N. Shirafuji, Y. Kanaoka, T. Tanaka, A. Nagata, N. Yoshida, Y. Urade, S. Ito, and O. Hayaishi. 1999. Lack of tactile pain (allodynia) in lipocalin-type prostaglandin D synthase-deficient mice. *Proc. Natl. Acad. Sci. USA* 96: 726–730.
8. Kostenis, E., and T. Ulven. 2006. Emerging roles of DP and CRTH2 in allergic inflammation. *Trends Mol. Med.* 12: 148–158.
9. Suzuki, F., H. Hayashi, and O. Hayaishi. 1986. Transport of prostaglandin D2 into brain. *Brain Res.* 385: 321–328.
10. Fitzpatrick, F. A., and M. A. Wynalda. 1983. Albumin-catalyzed metabolism of prostaglandin D2. Identification of products formed in vitro. *J. Biol. Chem.* 258: 11713–11718.
11. Kikawa, Y., S. Narumiya, M. Fukushima, H. Wakatsuka, and O. Hayaishi. 1984. 9-Deoxy-delta 9, delta 12-13,14-dihydroprostaglandin D2, a metabolite of prostaglandin D2 formed in human plasma. *Proc. Natl. Acad. Sci. USA* 81: 1317–1321.
12. Sawyer, N., E. Cauchon, A. Chateauneuf, R. P. Cruz, D. W. Nicholson, K. M. Metters, G. P. O'Neill, and F. G. Gervais. 2002. Molecular pharmacology of the human prostaglandin D2 receptor, CRTH2. *Br. J. Pharmacol.* 137: 1163–1172.

13. Liston, T. E., and L. J. Roberts, II. 1985. Transformation of prostaglandin D2 to 9 alpha, 11 beta-(15S)-trihydroxyprosta-(5Z,13E)-dien-1-oic acid (9 alpha, 11 beta-prostaglandin F2): a unique biologically active prostaglandin produced enzymatically in vivo in humans. *Proc. Natl. Acad. Sci. USA* 82: 6030–6034.
14. Beasley, C. R., C. Robinson, R. L. Featherstone, J. G. Varley, C. C. Hardy, M. K. Church, and S. T. Holgate. 1987. 9 alpha,11 beta-Prostaglandin F2, a novel metabolite of prostaglandin D2 is a potent contractile agonist of human and guinea pig airways. *J. Clin. Invest.* 79: 978–983.
15. Scher, J. U., and M. H. Pillinger. 2005. 15d-PGJ2: the anti-inflammatory prostaglandin? *Clin. Immunol.* 114: 100–109.
16. Forman, B. M., P. Tontonoz, J. Chen, R. P. Brun, B. M. Spiegelman, and R. M. Evans. 1995. 15-Deoxy-delta 12, 14-prostaglandin J2 is a ligand for the adipocyte determination factor PPAR gamma. *Cell* 83: 803–812.
17. Kliewer, S. A., J. M. Lenhard, T. M. Willson, I. Patel, D. C. Morris, and J. M. Lehmann. 1995. A prostaglandin J2 metabolite binds peroxisome proliferator-activated receptor gamma and promotes adipocyte differentiation. *Cell* 83: 813–819.
18. Ajuebor, M. N., A. Singh, and J. L. Wallace. 2000. Cyclooxygenase-2-derived prostaglandin D(2) is an early anti-inflammatory signal in experimental colitis. *Am. J. Physiol. Gastrointest. Liver Physiol.* 279: G238–G244.
19. Angeli, V., D. Staumont, A. S. Charbonnier, H. Hammad, P. Gosset, M. Pichavant, B. N. Lambrecht, M. Capron, D. Dombrowicz, and F. Trottein. 2004. Activation of the D prostanoid receptor 1 regulates immune and skin allergic responses. *J. Immunol.* 172: 3822–3829.
20. Monneret, G., S. Gravel, M. Diamond, J. Rokach, and W. S. Powell. 2001. Prostaglandin D2 is a potent chemoattractant for human eosinophils that acts via a novel DP receptor. *Blood* 98: 1942–1948.
21. Hammad, H., H. J. de Heer, T. Soullie, H. C. Hoogsteden, F. Trottein, and B. N. Lambrecht. 2003. Prostaglandin D2 inhibits airway dendritic cell migration and function in steady state conditions by selective activation of the D prostanoid receptor 1. *J. Immunol.* 171: 3936–3940.
22. Murata, T., K. Aritake, Y. Tsubosaka, T. Maruyama, T. Nakagawa, M. Hori, H. Hirai, M. Nakamura, S. Narumiya, Y. Urade, and H. Ozaki. 2013. Anti-inflammatory role of PGD2 in acute lung inflammation and therapeutic application of its signal enhancement. *Proc. Natl. Acad. Sci. USA* 110: 5205–5210.
23. Murata, T., M. I. Lin, K. Aritake, S. Matsumoto, S. Narumiya, H. Ozaki, Y. Urade, M. Hori, and W. C. Sessa. 2008. Role of prostaglandin D2 receptor DP as a suppressor of tumor hyperpermeability and angiogenesis in vivo. *Proc. Natl. Acad. Sci. USA* 105: 20009–20014.
24. Aritake, K., Y. Kado, T. Inoue, M. Miyano, and Y. Urade. 2006. Structural and functional characterization of HQL-79, an orally selective inhibitor of human hematopoietic prostaglandin D synthase. *J. Biol. Chem.* 281: 15277–15286.
25. Almishri, W., C. Cossette, J. Rokach, J. G. Martin, Q. Hamid, and W. S. Powell. 2005. Effects of prostaglandin D2, 15-deoxy-Delta12,14-prostaglandin J2, and selective DP1 and DP2 receptor agonists on pulmonary infiltration of eosinophils in Brown Norway rats. *J. Pharmacol. Exp. Ther.* 313: 64–69.
26. Spik, I., C. Brénuchon, V. Angéli, D. Staumont, S. Fleury, M. Capron, F. Trottein, and D. Dombrowicz. 2005. Activation of the prostaglandin D2 receptor DP2/CRTH2 increases allergic inflammation in mouse. *J. Immunol.* 174: 3703–3708.
27. Fujitani, Y., K. Aritake, Y. Kanaoka, T. Goto, N. Takahashi, K. Fujimori, and T. Kawada. 2010. Pronounced adipogenesis and increased insulin sensitivity caused by overproduction of prostaglandin D2 in vivo. *FEBS J.* 277: 1410–1419.
28. Satoh, T., R. Moroi, K. Aritake, Y. Urade, Y. Kanai, K. Sumi, H. Yokozeki, H. Hirai, K. Nagata, T. Hara, et al. 2006. Prostaglandin D2 plays an essential role in chronic allergic inflammation of the skin via CRTH2 receptor. *J. Immunol.* 177: 2621–2629.
29. Matsuoka, T., M. Hirata, H. Tanaka, Y. Takahashi, T. Murata, K. Kabashima, Y. Sugimoto, T. Kobayashi, F. Ushikubi, Y. Aze, et al. 2000. Prostaglandin D2 as a mediator of allergic asthma. *Science* 287: 2013–2017.
30. Murata, T., K. Aritake, S. Matsumoto, S. Kamauchi, T. Nakagawa, M. Hori, E. Momotani, Y. Urade, and H. Ozaki. 2011. Prostaglandin D2 is a mast cell-derived antiangiogenic factor in lung carcinoma. *Proc. Natl. Acad. Sci. USA* 108: 19802–19807.
31. Goetzl, E. J., and W. C. Pickett. 1981. Novel structural determinants of the human neutrophil chemotactic activity of leukotriene B. *J. Exp. Med.* 153: 482–487.
32. Kobayashi, K., Y. Tsubosaka, M. Hori, S. Narumiya, H. Ozaki, and T. Murata. 2013. Prostaglandin D2-DP signaling promotes endothelial barrier function via the cAMP/PKA/Tiam1/Rac1 pathway. *Arterioscler. Thromb. Vasc. Biol.* 33: 565–571.
33. Hirai, H., K. Tanaka, O. Yoshie, K. Ogawa, K. Kenmotsu, Y. Takamori, M. Ichimasa, K. Sugamura, M. Nakamura, S. Takano, and K. Nagata. 2001. Prostaglandin D2 selectively induces chemotaxis in T helper type 2 cells, eosinophils, and basophils via seven-transmembrane receptor CRTH2. *J. Exp. Med.* 193: 255–261.
34. Houle, F., and J. Huot. 2006. Dysregulation of the endothelial cellular response to oxidative stress in cancer. *Mol. Carcinog.* 45: 362–367.